Hydrogeochemical characteristics and evaluation of groundwater resources of Jilin Province, China

Zhaojun Zeng[1], Yueju Cui[1]*, Xiaocheng Zhou[1,2]*, Xiaodong Pan[3], Fengxia Sun[1], Yinan Liu[3], Jiao Tian[1], Miao He[1], Yongxian Zhang[1], Yucong Yan[1,2], Zhenyu Zou[1], Yuwen Wang[1], Bingyu Yao[1], Gaoyuan Xing[1] and Shihan Cui[1]

[1]United Laboratory of High-Pressure Physics and Earthquake Science, Institute of Earthquake Forecasting, China Earthquake Administration, Beijing, China, [2]School of Earth Sciences and Resources, China University of Geosciences, Beijing, China, [3]Jilin Earthquake Agency, Changchun, China

As one of China's nine border provinces, Jilin Province is an important window for China's "Belt and Road" to open up to the north, and an important channel for China's foreign trade and foreign exchanges. Therefore, understanding hydrogeochemical characteristics is very important for effective water resources management in Jilin Province. A total of 64 groundwater samples were collected from 32 monitoring Wells in Jilin Province. Use of hydrogeochemical analysis techniques, WQI index and human health risk index methods to assess hydrogeochemical processes and groundwater quality, including the determination of hydrogeochemical parameters, conventional ions, trace elements and stable isotopes (δD and δ^{18}O). The results show that the groundwater is slightly alkaline, the cations are mainly Na^+, Ca^{2+}, Mg^{2+}, and K^+, and the anions are mainly HCO_3^-, Cl^-, and SO_4^{2-}. Most of the groundwater samples belong to $Ca-HCO_3$ and $Na-HCO_3$ types, which are formed by the dissolution of calcite, dolomite, gypsum, silicates and carbonates. Stable isotope analysis shows that groundwater recharge in Jilin mainly comes from atmospheric precipitation at an altitude of 1,430~2,348 m. The strong correlation between trace elements indicates a common source. Most of the groundwater quality index (WQI) in the study area is Class I to Class III, and hazard quotient (HQ) and hazard index (HI) are both below 1. This indicates excellent water quality and minimal health risks associated with human consumption. It is worth noting that trace elements are enriched in the Tanlu fault zone. It provides scientific guidance for the utilization and allocation of groundwater resources in Jilin Province.

KEYWORDS

water chemistry, hydrogen and oxygen isotope, trace element, water quality evaluation, groundwater

1 Introduction

Groundwater is the primary source of freshwater worldwide, catering to the drinking and irrigation needs of billions of individuals. Compared to surface water, groundwater is generally considered to be a cleaner water resource. This is because groundwater is protected by different geological strata and is therefore less vulnerable to contamination from anthropogenic sources (An et al., 2023). In sub-humid and semi-arid areas, water quality directly affects human health, soil fertility, crop growth and the overall environment (Farhadkhani et al., 2018; Guo et al., 2022). Water quality is under threat from a number of sources around the world. In developing countries, where more than half of the world's population lives, about 20%—25% of people have access only to polluted drinking water (Yousefi et al., 2018; Adelodun et al., 2021). In arid regions, the main or even the only source

of fresh water available to mortals is groundwater. The advantages of groundwater resources over surface water include widespread distribution, consistent volume, and superior quality, rendering groundwater an essential water supply source, particularly in humid regions (Dash et al., 2019; Hao et al., 2023). Nevertheless, with the rapid development of society, the influence and interference of human activities on the hydrosphere are intensifying. For example, human sewage discharged daily into groundwater has increased significantly. Large-scale pumping and irrigation could drastically alter the hydrodynamic conditions and environment of aquifers (Wang et al., 2022). In the 21st century, the global recognition of groundwater management's significance has grown. The chemical makeup of groundwater has close links to the type of aquifer, the duration of water-rock interaction, and the influences of natural or anthropogenic activities (Maliva, 2020).

Water quality is crucial for human well-being and health. It must be taken into account to ensure that water resources are safe for consumption and use. Groundwater quality and its processes can be assessed over time and space using hydrogeochemical analysis. According to the hydrogeochemical analysis technology, Piper three-line diagram and Gibbs diagram are used to identify the evolution of the chemical composition of groundwater (Li et al., 2020; Zhong et al., 2022). These analytical methods have been extensively used to evaluate groundwater quality and hydrogeochemical changes of pollutants, such as fluoride (Qiu et al., 2023), nitrate (Li et al., 2023), and trace elements (Bodrud-Doza et al., 2019; Aithani et al., 2020). Moreover, numerous countries across the globe have undertaken assessments to evaluate the presence of trace elements in water quality and their potential risks to human health. In the 1960s, Horton introduced the earliest water quality index (WQI), and numerous techniques for assessing water quality have been developed since (Adimalla and Taloor, 2020). Although water quality assessment methods have developed rapidly in recent years, human health risk assessment still relies heavily on the models proposed by the US Environmental Protection Agency (USEPA) or their improvements (Zhang et al., 2018).

The quality of groundwater for drinking water in the Nur region of southern Ghana has been assessed using the WQI (Adimalla and Qian, 2019). The assessment of the WQI was carried out in the Upper Awash River Basin in Ethiopia. Based on the results of water chemical analysis, the samples were classified into three WQI categories: excellent (58.82%), good (35.29%), and poor (5.88%) (Haji et al., 2021). Groundwater in industrialized and densely populated areas of southern India has a high level of nitrate contamination, rendering it unsuitable for drinking. Nitrate levels are elevated in semi-arid regions, requiring treatment before consumption, particularly for children who are more vulnerable to non-carcinogenic hazards. Inadequate sanitation facilities, insufficient wastewater treatment, and seepage runoff have a detrimental effect on water quality in Srikakulam district of Andhra Pradesh (Nadikatla et al., 2020; Soujanya Kamble et al., 2020; Panneerselvam et al., 2023). Studies in Pakistan found that heavy metal contamination in food crops poses health risks to humans and animals. Thereby mandating the implementation of measures to minimize pollution. The assessment of groundwater showed that 3.23% of samples were excellent, 93.54% were good, and 3.23% were

poor according to water quality standards. Geologic processes and human activities play a significant role in the chemical properties of groundwater (Kawo and Karuppannan, 2018; Khaliq et al., 2022). The water quality in the Mesta River catchment, Bulgaria, was assessed using a novel approach combining CCME WQI and SOM, enabling precise evaluation by water management authorities (Yotova et al., 2021). The water quality of the Turnasuyu Stream was evaluated, revealing very good quality with low levels of trace elements, posing no health risks (Ustaoglu et al., 2020). Water quality, concentrations, and health risks of heavy metals in eight major lakes in Kenya were evaluated, with varying levels of contamination identified and the need for remediation policies highlighted (Githaiga et al., 2021). Groundwater quality in a semi-arid area of China was assessed, with suitable drinking water sources identified and health risks due to contamination highlighted (Zhang et al., 2020). An analysis of groundwater in Shandong Province, China revealed conflicting results between water quality and health risk assessment, emphasizing the necessity of adjusted standard (Liu et al., 2021). The water quality of rivers in the Tibetan Plateau was compared to global averages, Chinese national standards, and World Health Organization drinking water guidelines. Most rivers were found to be uncontaminated, but some basins showed excessive concentrations of toxic elements, warranting long-term monitoring (Qu et al., 2019).

Over the past decades, numerous scholars have conducted in-depth research in the Jilin. For instance, the groundwater in Da'an City, Jilin Province, was evaluated based on the Water Level Sequence Data and the Mine Groundwater Sustainability Index (MGSI). It is suggested by the study that future water resource management should consider replacing groundwater with surface water or other water sources to reduce groundwater extraction (Fang et al., 2022). Assessments of groundwater in Jilin Province indicated low pollution risks and suitability for drinking (Huan et al., 2018). The majority of the underground water in the Jilin section of Songhua River was found to be suitable for drinking, according to the WQI, Health Quotient (HQ), and Health Index (HI) evaluation methods (Tong et al., 2021). Furthermore, the WQI of Dehui City, Jilin Province, was conducted using fuzzy comprehensive evaluation and multivariate statistical analysis, which indicated good water quality (Chai et al., 2020). Analysis of groundwater samples in Jilin Province suggested their suitability for irrigation (Xiao et al., 2016). Additionally, the groundwater hydrochemistry of multiple aquifers in Qian'an City, Jilin Province, was studied to evaluate the non-carcinogenic health risks associated with groundwater (Adeyeye et al., 2021). The impact of the natural environment and human activities on Fe and Mn levels in Changchun City's groundwater was investigated, identifying their sources and the role of anthropogenic fertilization (Zhang et al., 2021). Furthermore, a groundwater flow model was established using GMS to gain better understanding of the groundwater system responsible for the Jilin City area (Qiu et al., 2015).

Despite the significant progress achieved in previous studies on groundwater, the scope and comprehensiveness of this research are broader. This study combines hydrogeochemical analysis with water quality assessment to provide a comprehensive evaluation of groundwater in Jilin Province. The motivation behind this study is driven by concerns for environmental protection, water resource

management, as well as the impact of groundwater on human health and ecosystems. By investigating the hydrogeochemical properties and evaluating the water quality of groundwater in Jilin Province, we can gain a comprehensive understanding of groundwater quality in the region. This includes identifying the types and concentrations of dissolved substances in the water and assessing whether the groundwater meets relevant water quality standards and criteria. This research presents empirical evidence that can be utilized to manage and safeguard groundwater in Jilin Province. It furnishes valuable insight to residents and decision-makers to ensure the sustainable utilization and safety of groundwater.

2 Geological profiles

Jilin Province (Figure 1), situated in the heart of northeastern China, lies between 121°38′-131°19′ east longitude and 40°50′-46°19′ north latitude. Comprising nine prefecture-level administrative regions, it hosts a large population within a total area of 18.74×10^4 km^2, accounting for approximately two percent of the country's overall area. Jilin Province borders Heilongjiang and Liaoning Provinces. It has a temperate continental monsoon climate with rainy summers and snowy winters. The annual temperature ranges from -2 to $6°C$, and average precipitation is 400–600 mm, varying from southeast to northwest (Adeyeye et al., 2021; Chen et al., 2021). Jilin Province is home to five major river systems: Songhua River, Liao River, Tumen River, Yalu River, and Suifen River (Jilin Provincial Environmental Protection Bureau, 2022). Among them, Songhua, Tumen, and Yalu River systems originate from Changbai Mountain, radiating outwards. The Liao River system originates from Mount Guangtou in Pingquan County, Hebei Province, and flows into the western and eastern parts of Jilin Province as the tail section of the West Liao River and most of the East Liao River, as well as parts of the Zhaosutai River. Suifen River originates from the northern side of the Dalongce range in Wangqing County, Jilin Province, enters Heilongjiang Province, and finally empties into the Sea of Japan through Russia. The distribution of annual runoff of Jilin Province's rivers ranges from the Changbai Mountain area to the west, extending to the hilly and plain areas, and the depth of runoff decreases along with the elevation and precipitation (Chen et al., 2021). In summary, Jilin Province possesses abundant water resources but also faces water quality issues and challenges that require proper management and protection.

Jilin's primary rock is magmatic, dominated by granites in eastern mountainous areas like Jiaohe and Wangqing. Residual slope deposits from weathered granite are found in Panshi, Liaoyuan, and other places. Lava platforms in Changbai Mountain and Dunhua consist mainly of different types of basalts, while Jurassic volcanic rocks are in Wangqing and north Dunhua (Huan et al., 2018). Jilin Province is traversed by three distinct geological units, extending from southeast to northwest: the Changbai Mountain Range, the Songliao Plain, and the Greater Khingan Mountains (Cai et al., 2003). Mineralization levels gradually increase from east to west. In the eastern region, which includes the Greater Khingan Mountains and the Changbai Mountain hilly area, rainfall is abundant but groundwater conditions are unfavorable.

The hilly terrain of the Greater Khingan Mountains favors the occurrence of groundwater, but precipitation is relatively low. The northwestern region is affected by climate, human activities, land desertification, salinization, and groundwater pollution, resulting in deteriorating water quality and high mineralization levels (Liu et al., 2017).
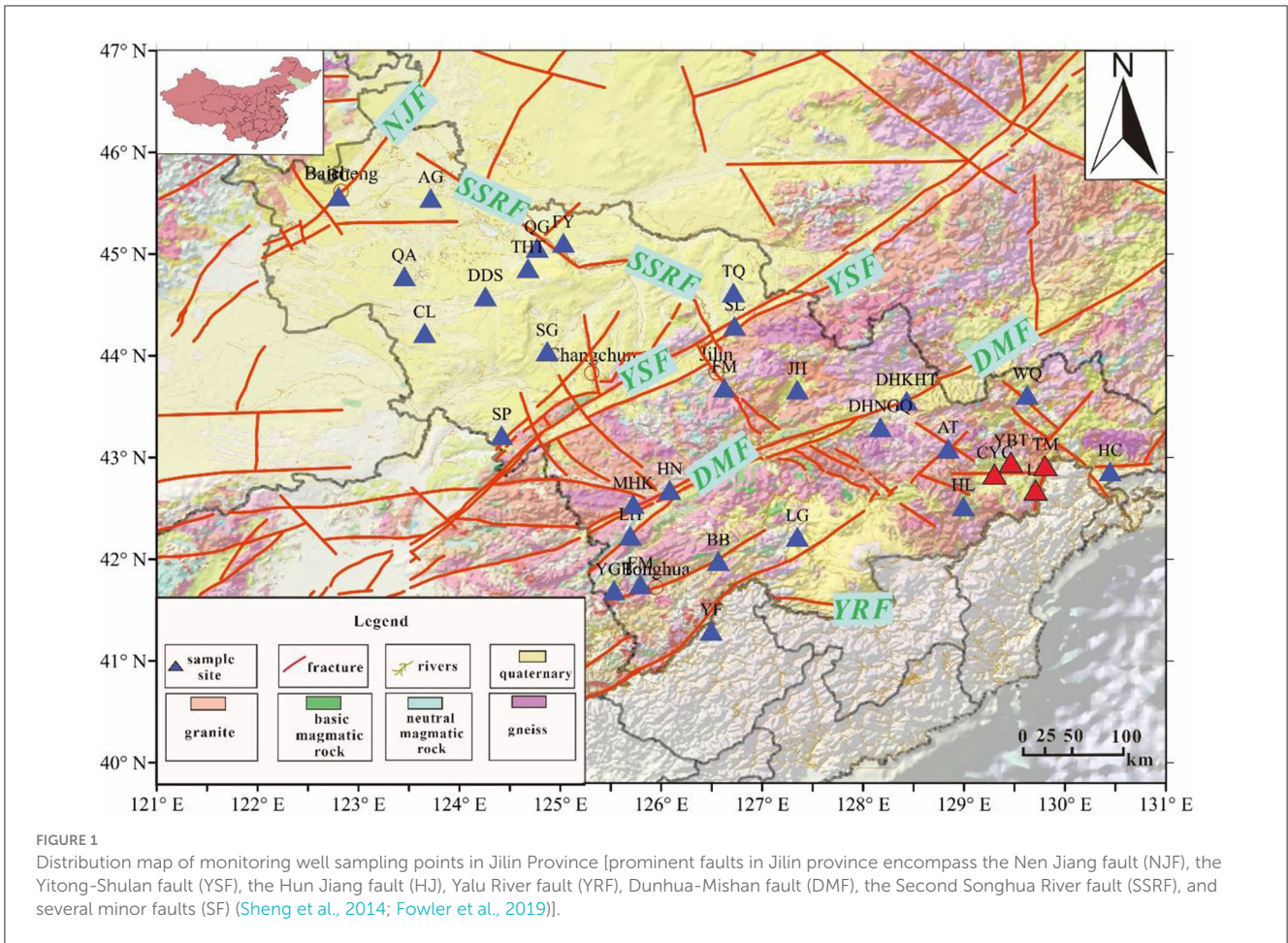
Given the spatial distribution and structural characteristics of the sampling points in the study area, the sample sites are segmented into three divisions: plain area, fault zone area, and volcanic area. Sites QA, AG, CL, DDS, THT, SG, TQ, and JH lie within the plain region, while YBT, CYC, LY, and TM belong to volcanic areas. The remaining sample sites fall within the fault zone.

3 Sampling and methods

3.1 Groundwater samples collection and analysis

During 2016, 64 groundwater samples were collected from 32 locations in the study area. The samples, classified as shallow groundwater, were gathered from observation wells at depths ranging from 0 to 20 m. The sample sites, including AG, AT, BB, BC, CL, CYC, DDS, DHKHT, DHNGQ, EM, FM, FY, HC, HL, HN, JH, LG, LH, LJ, MHK, QA, QG, SG, SL, SP, THT, TM, TQ, WQ, YBT, YF, and YGB, are illustrated in Figure 1 and detailed in Table 1. Groundwater samples were filtered using a 0.45 μm filter and collected in 50 ml polyethylene bottles. At least four bottles were collected per water sample and stored in a refrigerator with ice to maintain a constant temperature of 4°C during storage (Adimalla and Taloor, 2020). To ensure sample integrity, each bottle was soaked in ultra-pure water for 3 days and thrice rinsed with groundwater prior to sampling. Furthermore, after collecting water, 14 M HNO$_3$ was gradually added to acidify the sample to a pH < 2. The bottle was then sealed to prevent exposure to light and to ensure that the sample is not exposed to air until analysis. All water samples were processed within 1 week.

The collected water samples were transported to the laboratory for compositional analysis, focusing on their hydrogeochemical and isotopic characteristics. The chemical composition of the water, encompassing cations (Na$^+$, K$^+$, Ca^{2+}, and Mg^{2+}) and anions (Cl$^-$, Br$^-$, SO$_4^{2-}$, and NO$_3^-$), was determined by Dionex ICS-900 ion chromatograph with AS40 automatic sampler provided by the Key Laboratory of Earthquake Prediction of China Earthquake Administration, with the reproducibility within ±2% a limit of detection of 0.01 mg/L. The concentrations of HCO$_3^-$ and CO$_3^{2-}$ were determined using 0.05 mol/L HCl, 0.1% methyl orange, and 1% phenolphthalein procedures with a ZDJ-100 potentiometric titrator, which exhibited a reproducibility within ±2%. The analysis of the trace elements was completed at the Test Center of the Institute of Nuclear Industry Geology, using an element-type inductively coupled plasma mass spectrometer ICP-MS. Hydrogen and oxygen isotopes were analyzed with MAT 253, and Vienna Standard Mean Ocean Water (V-SMOW) served as the reference sample. The δ^{18}O and δD values were measured with an accuracy of ±0.2% (2SD) and ±1% (2SD), respectively.

FIGURE 1
Distribution map of monitoring well sampling points in Jilin Province [prominent faults in Jilin province encompass the Nen Jiang fault (NJF), the Yitong-Shulan fault (YSF), the Hun Jiang fault (HJ), Yalu River fault (YRF), Dunhua-Mishan fault (DMF), the Second Songhua River fault (SSRF), and several minor faults (SF) (Sheng et al., 2014; Fowler et al., 2019)].

$$ib\,(\%) \;=\; \frac{\sum cations - \sum anions}{0.5(\sum cations + \sum anions)} \times 100 \qquad (1)$$

When the anions and cations balance error is less than ±5%, the determination results of the main ions in water can be used to analyze the hydrogeochemical characteristics (Bianchini et al., 2005).

3.2 Mineral saturation states

The saturation index method is widely used to assess and investigate the mineral saturation state in relation to groundwater (Giggenbach, 1988). The saturation index method is defined as follows:

$$SI \;=\; lg\,(IAP/K_{sp})$$

where K_{sp} represents the equilibrium constant of the mineral dissolution reaction, and IAP denotes the active product of related ions in mineral dissolution reactions. According to the solubility product rule:

When SI > 0, compounds originate from groundwater deposition.

When SI = 0, the dissolution and precipitation of the compound are in equilibrium.

When SI < 0, compounds are unsaturated in groundwater and have a tendency to dissolve.

3.3 Water quality index

The WQI is the optimal environmental standard and one of the most effective tools. WQI provides a single value that represents the overall water quality at a specific location and helps in specifying environmental management strategies to control groundwater pollution (Soujanya Kamble et al., 2020). To assess the cumulative impacts of various harmful elements on aquatic ecosystems, a comprehensive pollution index known as the WQI was employed. The WQI is calculated using the following method (Qu et al., 2019):

$$WQI = \frac{1}{n} \sum_{i=1}^{n} Ai = \frac{1}{n} \sum_{i=1}^{n} Ci/Qi$$

In the formula, Ci represents the concentration of element I detected in the water, while Qi represents the water quality standard limit for element I. The variable n indicates the number of elements. The WQI is divided into four categories:

TABLE 1 Location of monitoring well in Jilin Province.

Sample number	Longitude (°)	Latitude (°)
AG	123.76	45.60
AT	128.87	43.13
BB	126.60	42.02
BC	122.85	45.62
CL	123.70	44.27
CYC	129.33	42.88
DDS	124.30	44.63
DHKHT	128.46	43.60
DHNGQ	128.20	43.34
EM	125.83	41.79
FM	126.66	43.73
FY	125.07	45.16
HC	130.47	42.91
HL	129.02	42.56
HN	126.12	42.72
JH	127.38	43.71
LG	127.38	42.26
LH	125.73	42.27
LJ	129.73	42.71
MHK	125.76	42.58
QA	123.50	44.83
QG	124.81	45.11
SG	124.91	44.09
SL	126.76	44.34
SP	124.46	43.26
THT	124.72	44.91
TM	129.83	42.96
TQ	126.75	44.67
WQ	129.65	43.66
YBT	129.49	43.00
YF	126.53	41.33
YGB	125.57	41.73

1. Category I (almost uncontaminated): WQI ≤ 1.
2. Category II (mildly contaminated): 1 < WQI ≤ 2.
3. Category III (moderately contaminated): 2 < WQI ≤ 3.
4. Category IV (heavily contaminated): WQI > 3 (Qu et al., 2019).

3.4 Human health risk

Common exposure pathways for human beings are typically considered to be direct ingestion and dermal absorption by the skin (through activities such as showering/bathing and swimming) (Gao et al., 2019; Tong et al., 2021). The non-carcinogenic human health risks of ingestion (HQingestion) and dermal contact (HQdermal) were used to calculate the hazard quotient (HQ) (Githaiga et al.,

2021; Tong et al., 2021). The steps outlined by US EPA (2004) were followed in the calculation of HQingestion and HQdermal risks.

$$ADDingestion = \frac{Cw \times IR \times EF \times ED}{BW \times AT}$$

$$ADDdermal = \frac{Cw \times SA \times Kp \times ET \times EF \times ED \times 10^{-3}}{BW \times AT}$$

Among them, the average daily dose of intake and skin adsorption is represented by $ADD_{ingestion}$ and ADD_{dermal}, measured in μg/kg/day. C_w is the average concentration of trace elements in various water samples, expressed in μg/L. IR refers to the ingestion rate, which is 2.0 L/day for adults and 0.64 L/day for children. EF indicates the exposure frequency, calculated as 350 days/year. The duration of ED exposure is 30 years for adults and 6 years for children. BW represents the average weight, with adults at 70 kg and children at 15 kg. AT stands for the average time, where for non-carcinogens, AT = ED × 365 days/year, and for carcinogens, AT = 365 days/year × 70 years. SA denotes the exposed skin area, which is 18,000 cm^2 for adults and 6,600 cm^2 for children. ET indicates the exposure time, with adults at 0.58 and children at 1 h per day. These exposure parameters were referenced from the US EPA (2004), Zhang et al. (2020) and Haji et al. (2021). Kp (cm/h) is the Dermal Permeability Constant expressed in cm/h. The values are as follows: 1.0×10^{-3} for Al, As, B, Ba, Cd, Mo, Se, Sr, Mn, Fe, Cu, and V; 2.0×10^{-3} for Cr; 4.0×10^{-4} for Co; 1.0×10^{-4} for Pb; 2.0×10^{-4} for Ni; and 6.0×10^{-4} for Zn (Ustaoglu et al., 2020; Githaiga et al., 2021).

The evaluation formula of potential non-carcinogenic risk is as follows:

$$HQ = \frac{ADD}{RfD}$$

$$RfD_{dermal} = RfD \times ABSg$$

$$HI = \sum (HQ_{ing} + HQ_{dem}).$$

Among the variables mentioned, HQ represents the hazard quotient, which is a dimensionless measure of the potential hazard through ingestion or skin absorption. RfD refers to the reference dose for oral toxicity of a specific metal. ABSg is the gastrointestinal absorption factor, expressed as a dimensionless value, with reference values derived from the US EPA's Risk-Based Concentration Table. HI stands for the hazard index, which is a dimensionless value, indicating the potential non-carcinogenic risk associated with all heavy metals. Adverse health effects may occur when HQ or HI values exceed 1, whereas values below 1 indicate no adverse effects on human health (US EPA, 2004). The classification of HI is as follows: HI < 0.1 indicates a negligible non-carcinogenic risk, 0.1 ≤ HI < 1 suggests a low non-carcinogenic risk, 1 ≤ HI <

4 implies a moderate non-carcinogenic risk, and HI $\geq$ 4 denotes a high non-carcinogenic risk (Tong et al., 2021).

Software packages such as The Origin 2021b, Surfer 17.1, and Grapher 17.3 were employed for the generation of plots. By utilizing these tools, plots were efficiently generated and information was effectively presented through advanced data visualization and graphical analysis features.

4 Results

The typical concentrations of conventional constituents within the groundwater samples were calculated, and their average values represent the overall state of the standard ion concentration indices throughout the entirety of the study (refer to Supplementary Table 2). The mean cation concentration in the groundwater system is ordered from highest to lowest as $Na^+ > Ca^{2+} > Mg^{2+} > K^+$, with Na^+ being the most prevalent cation. Conversely, the average anion concentration ranks as $Cl^- > HCO_3^- > SO_4^{2-}$, with Cl^- and HCO_3^- predominating as the most common anions in the groundwater. The total dissolved solids (TDS) concentrations across the three groundwater systems exhibited variation, ranging between 6.48 and 210.99 mg/l in the volcanic area, 61.69 and 7,441.63 mg/l in the fault zone, and 126.11 and 6,279.65 mg/l in the plain area. The pH values for these groundwater systems spanned from 7.42 to 8.21, 7.14 to 9.62, and 7.72 to 9.24 respectively, indicating that the groundwater was generally weakly alkaline.

5 Discussion

5.1 Stable isotopes

It is known that the global meteoric water line (GMWL) can be expressed as $\delta^2H = 8 \times \delta^{18}O + 10$ (Craig, 1961), and the local meteoric water line (LMWL) specific to Jilin is $\delta^2H = 8.04 \times \delta^{18}O + 6.88$ (Liu et al., 1997). As can be observed in Figure 2, the isotope values in the study area deviate from GMWL and LWML.

Groundwater samples in fault area and plain area are distributed on both sides of GMWL and LMWL, indicating that they are replenished by atmospheric precipitation. Oxygen isotopes can be found drifting to the right of the atmospheric precipitation line in Region1. This may be due to the isotope imbalance between atmospheric precipitation and rocks, and the oxygen isotope exchange between water and rock minerals, resulting in the enrichment of heavy isotopes in groundwater (Strohmenger et al., 2022; Zhou et al., 2022a,b). Oxygen isotopes in Region 2 drift to the left of the precipitation line, indicating that the precipitation in the study area may have experienced certain evaporation before reaching the surface, resulting in light oxygen isotope values (Ren et al., 2018; Al-Gburi et al., 2022; Su et al., 2022). The oxygen isotope values in volcanic areas are obviously biased and are distributed in the upper right of the precipitation line. This suggests that Changbai Mountain snowmelt water may serve as an additional source of recharge, indicating the possibility of other sources besides atmospheric precipitation (Qiao et al., 2019; Li et al., 2022; Strohmenger et al., 2022). With the increase in temperature and

evaporation, the $\delta^{18}O$ of snowmelt water becomes more and more abundant, the recharge elevation is high and the recharge path is long, which leads to the slow runoff process and intensifies the interaction between water and surrounding rock. In addition, the main source of water vapor in the study area is brought by the Pacific monsoon, and is transported over long distances and continuously depleted, so the hydrogen and oxygen isotope values in the Changbai Mountain volcanic area are heavy (Feng et al., 2022; Li et al., 2022).

Because all water samples in the study area are from atmospheric water, the elevation effect of δ^2H and $\delta^{18}O$ in atmospheric water can be used to estimate the recharge altitude of water samples in the study area. Therefore, use Formula 1 to estimate the height of the recharges, ranging from 1,430 to 2,348 m (Table 2).

(1) Elevation effect formula of the value of δ^2H precipitation in China (Zhou et al., 2022a,b):

$$\delta^2H = -0.03H - 27 \qquad (2)$$

5.2 Hydrochemical characteristics of groundwater

The concentration ratios of cations ($K^+ + Na^+$, Mg^{2+}, and Ca^{2+}) and anions (Cl^-, SO_4^{2-}, and HCO_3^-) in water samples collected from 32 stations were analyzed. The prevalent chemical types of groundwater are $Ca\cdot Na\text{-}HCO_3$ and $Na\text{-}HCO_3$, followed by $Na\text{-}HCO_3\cdot Cl$ and $Na\text{-}Cl$. Figure 3, which displays a Piper diagram using the hydrogeochemical data, indicates that the chemical types of groundwater samples vary spatially in this area, likely owing to local geological structures, properties of the surrounding rocks, and hydrothermal conditions (Deshaee et al., 2020; Qi and Tong, 2023). As can be seen from Figure 3, most of the points in the plain area are concentrated in zone 6, where the water chemical type is $Na\text{-}HCO_3$. The points in the volcanic area are basically concentrated in region 3, and the hydrochemical type is $Ca\cdot Na\text{-}HCO_3$. The sites in the fault zone are concentrated in region 1 and 4, which may be mainly attributed to the dissolution of calcite, dolomite, and other minerals in the surrounding rocks, thereby enriching the water with Ca and HCO_3 ions (Guo et al., 2018; Lei et al., 2022).

It can be seen from Figure 4A that the ratio of Ca^{2+} to Mg^{2+} is >1 in basically all regions, indicating that Ca^{2+} treatment comes not only from calcite, gypsum, and cation exchange (Ndoye et al., 2023). In Figure 4B, it can be found that the ratio of Ca^{2+} to HCO_3^- is ~1 in the fault area, 1/2 in the volcanic area, and 1/4 in the plain area. This indicates that Ca^{2+} and HCO_3^- in the fault zone are derived from the dissolution of dolomite and calcite, in the volcanic area they are completely derived from the dissolution of calcite, and in the plain area from the dissolution of dolomite (Heiß et al., 2020; Liu et al., 2022) As can be seen from Figure 4C, the groundwater sampling points in the fault zone and volcano area are mainly distributed on the line of $\gamma(Ca^{2+} + Mg^{2+})/\gamma(SO_4^{2-} + HCO_3^-) = 1$, indicating that Ca^{2+}, Mg^{2+}, SO_4^{2-} and HCO_3^- in the groundwater in these regions are mainly derived from the dissolution of dolomite
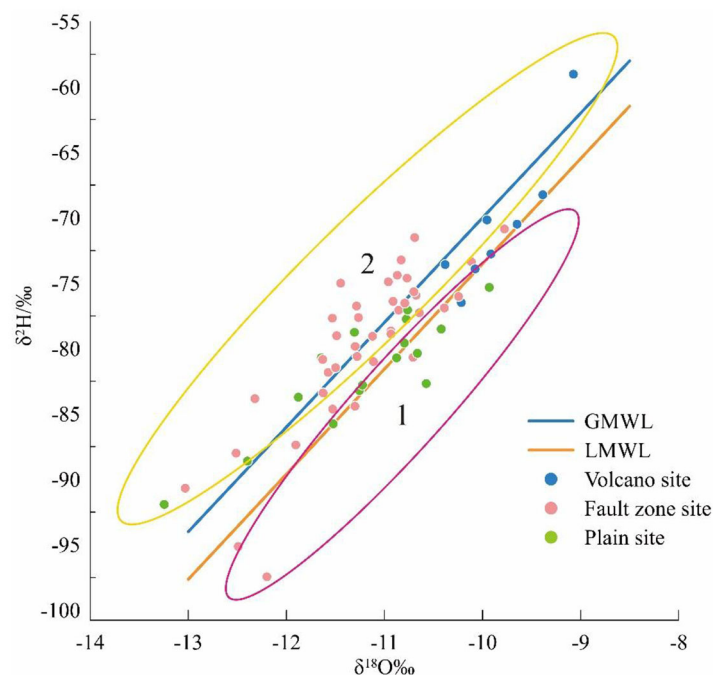
FIGURE 2
Relationship between δ^2H and $\delta^{18}O$ in water bodies in different regions.

and gypsum. The sampling points of groundwater in the plain area fall below the straight line, which shows that Ca^{2+}, Mg^{2+}, SO_4^{2-} and HCO_3^- in the groundwater in the plain area mainly come from the dissolution of sulfate and silicate (Ndoye et al., 2018, 2023).

Groundwater of different types shows differences and similarities in its chemical composition characteristics, reflecting the variations in groundwater hydrogeochemical formation mechanisms. Gibbs diagrams and rock end-member element ratio diagrams can be used to analyze the hydrogeochemical origins of various groundwater. The Gibbs diagram is widely used to identify the natural mechanisms (rock weathering, precipitation, and evaporation) that affect the dissolved chemical constituents of surface water and groundwater (Gu et al., 2022; Bian et al., 2023). Based on Figures 5A, B, it can be observed that the majority of sampling points in the study area are distributed in the weathered rock zone and are far from the influence of atmospheric rainfall. This indicates that the major ion composition of the groundwater in the study area is primarily controlled by rock weathering processes. This can be attributed to the relatively deep groundwater level in the study area, which is less influenced by atmospheric rainfall and evaporation (Adeyeye et al., 2021). However, due to the influence of structural conditions, there is development of fractured lava, providing favorable conditions for rock weathering. Basically, most of the water samples in the plain area and the volcanic area, as well as some water samples points in the fault zone fall outside Gibbs, which indicates that it may be affected by cation exchange. The results indicated that Ca^{2+} and Mg^{2+} in aqueous medium were replaced by Na^+ and K^+ (Zhou et al., 2022a,b).

According to Figure 5, the distribution of water sample points in the study area is centered on the distribution of silicate rock and

extends to the two ends of evaporative rock and carbonate rock. It is worth noting that the water sample points in the volcanic area and plain area are more concentrated in the end elements of the silicate rock, indicating that the chemical characteristics of the groundwater in the volcanic area and plain area are mainly controlled by the weathering of the silicate rock. The water samples in the fault zone area are scattered in the figure, which indicates that the groundwater water sample points are mainly controlled by carbonate rock and silicate rock, and the evaporative rock salt is less controlled (Adeyeye et al., 2021; Zhou et al., 2023).

5.3 Mineral saturation states (SI)

According to the simulation results, it can be seen that Anhydrite, Aragonite, Calcite, Dolomite, Fluorite, Gypsum, and Halite in groundwater are all in an unsaturated state (Figure 6), which indicates that most of the elements come from rock differentiation.

As can be seen from the Table 3, the maximum SI value of Anhydrite, Aragonite, Calcite, Dolomite, Fluorite, Gypsum, and Halite in the volcanic area is lower than that in the fault zone and plain area. A higher SI value indicates that these minerals are higher in content and stay in the aquifer for a long time (Wang et al., 2022). This phenomenon might denote variations in the attributes of the adjacent rock, suggesting that there hasn't been any establishment of ionic equilibrium between the water and the rock, that the dissolution process is still ongoing, or that a blend of hot and cold water is occurring (Zhou et al., 2022a,b).

TABLE 2 Elevation of groundwater replenishment in Jilin Province.

Sample site	May		Recharge elevation (m)	August		Recharge elevation (m)
	δ^2H (‰)	$\delta^{18}O$ (‰)		δ^2H (‰)	$\delta^{18}O$ (‰)	
AG	−85.76	−11.52	1,959	/	/	/
AT	−79.06	−11.12	1,735	−80.67	−11.38	1,789
BB	−83.83	−12.32	1,894	−83.54	−11.24	1,885
BC	−84.41	−11.3	1,914	−80.67	−11.38	1,789
CL	−78.51	−10.42	1,717	−79.98	−11.34	1,766
CYC	−70.49	−9.65	1,450	−76.49	−10.45	1,650
DDS	−83.21	−11.26	1,874	−79.98	−11.34	1,766
DHKHT	−80.6	−11.28	1,787	−75.55	−10.38	1,618
DHNGQ	−81.82	−11.57	1,827	/	/	/
EM	−74.39	−10.87	1,580	−72.45	−10.26	1,515
FM	−77.06	−10.85	1,669	−84.64	−10.96	1,921
FY	−87.37	−11.9	2,012	−84.64	−10.96	1,921
HC	−77.68	−11.53	1,689	/	/	/
HL	−80.67	−10.71	1,789	−80.1	−10.62	1,770
HN	/	/	/	−75.37	−10.03	1,612
JH	−83.72	−11.88	1,891	−80.79	−11.11	1,793
LG	−90.68	−13.03	2,123	−87.9	−12.01	2,030
LH	−77.13	−11.11	1,671	−76.48	−10.5	1,649
LJ	−76.49	−10.22	1,650	−73.41	−9.39	1,547
MHK	−73.37	−10.11	1,546	−71.78	−9.43	1,493
QA	−82.79	−11.22	1,860	−80.08	−10.46	1,769
QG	−97.45	−12.2	2,348	−95.84	−11.45	2,295
SG	−91.91	−13.25	2,164	−88.16	−11.7	2,039
SL	−78.65	−10.93	1,722	−76.15	−10.39	1,638
SP	−81.46	−11.5	1,815	−78.78	−10.91	1,726
THT	−77.74	−10.78	1,691	−74.89	−9.87	1,596
TM	−73.58	−10.38	1,553	−71.48	−9.88	1,483
TQ	−79.57	−10.8	1,752	−79.2	−10.14	1,740
WQ	−76.9	−10.39	1,663	−75.51	−10.34	1,617
YBT	−72.76	−9.91	1,525	−69.91	−9.4	1,430
YF	−76.02	−10.24	1,634	−74.77	−10.25	1,592
YGB	−74.89	−10.96	1,596	−71.86	−10.04	1,495

There exists a dynamic disequilibrium state between calcite and dolomite in the water bodies (Figure 7). Calcite displays an undersaturated state in ordered dolomite, indicating that the dissolution rate of calcite in the water is higher than its precipitation rate. In disordered dolomite, calcite is slightly undersaturated but closer to saturation compared to ordered dolomite (Zhou et al., 2022a,b). Under high-temperature conditions, ordered dolomite exhibits an unstable phase due to its structure's susceptibility to change at high temperatures. The undersaturated state may be linked to the presence of non-stoichiometric dolomite, where the chemical composition is not entirely matched. Additionally, increased cation disorder also affects the stability of ordered dolomite, leading to its undersaturated state. The maintenance of this undersaturated state is closely linked to the associated kinetic processes (Apollaro et al., 2020).

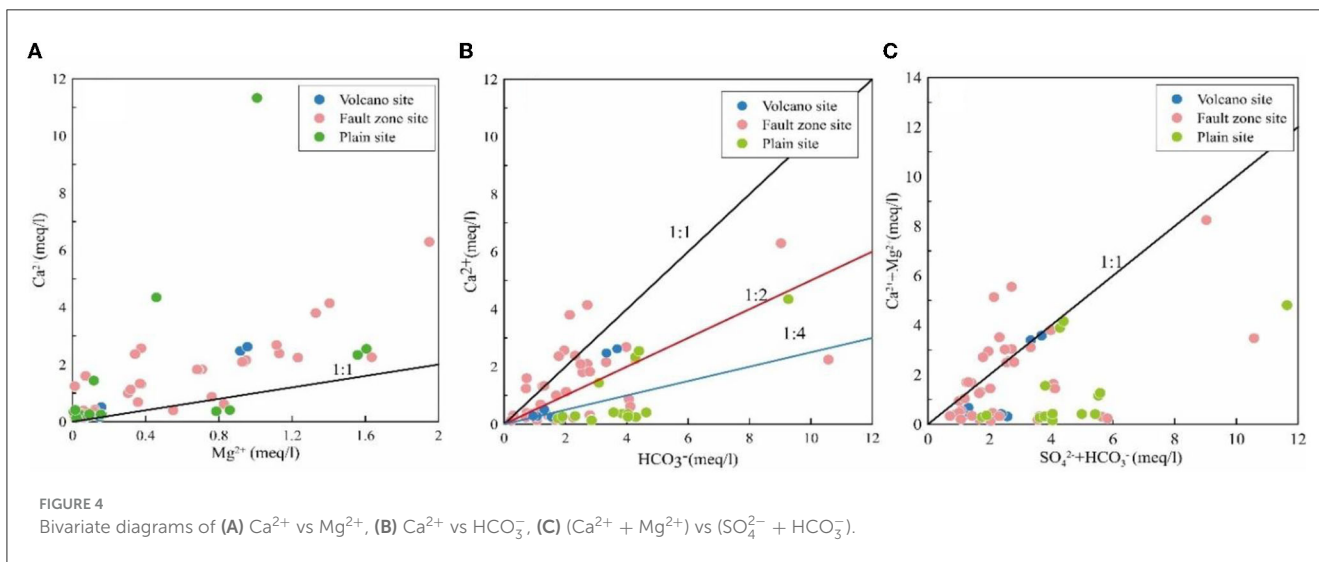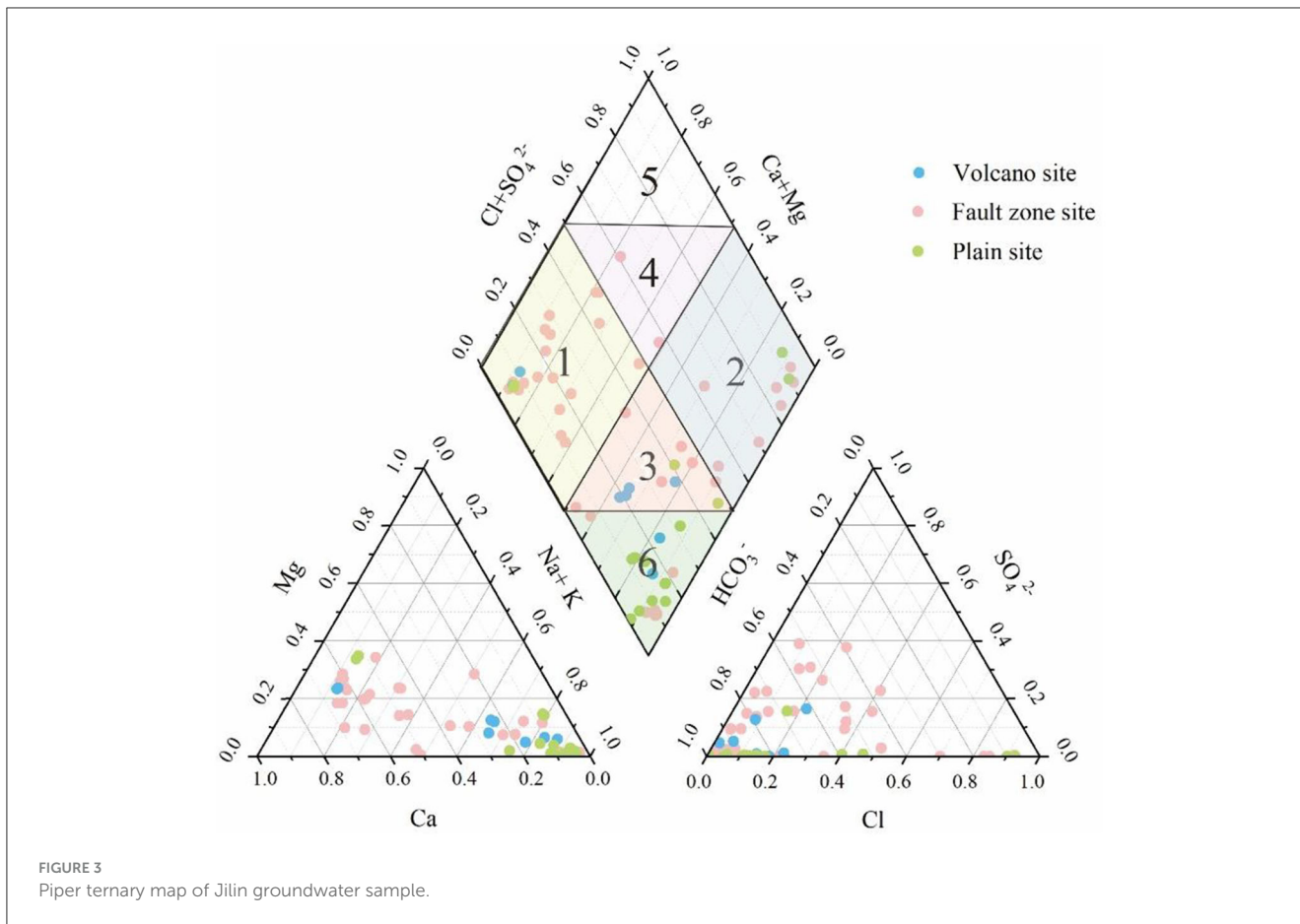TABLE 3 Water sample mineral saturation index (SI).

	Anhydrite	Aragonite	Calcite	Dolomite	Fluorite	Gypsum	Halite
CYC	−8.28	−4.88	−4.73	−9.34	−6.2	−8.06	−11.02
LJ	−7.77	−3.00	−2.85	−5.42	−6.34	−7.55	−10.6
TM	−5.62	−4.62	−4.47	−9.07	−6.11	−5.4	−10.81
YBT	−4.99	−3.26	−3.12	−6.37	−5.76	−4.77	−11.36
AT	0.00	−3.79	−3.65	−6.46	0.00	0.00	0.00
BB	−5.51	−4.81	−4.67	−9.31	−6.72	−5.29	−10.5
BC	−5.53	−3.56	−3.42	−8.84	−5.67	−5.31	−10.8
DHKHT	−5.55	−3.33	−3.19	−6.43	−5.97	−5.33	−11.17
DHNGQ	−5.97	−3.41	−3.27	−6.59	−6.24	−5.75	−12.15
EM	−4.21	−3.15	−3.01	−6.21	−5.96	−3.99	−9.91
FM	−4.73	−3.58	−3.44	−7.37	−3.94	−4.51	−10.49
FY	−8.2	−6.80	−6.65	−13.19	−6.28	−7.98	−8.88
HC	−6.04	−4.63	−4.49	−9.27	−3.99	−5.82	−10.56
HL	−4.7	−3.32	−3.18	−6.21	−5.22	−4.48	−10.78
HN	−5.08	−3.87	−3.72	−7.71	−4.11	−4.86	−11.11
LG	−5.82	−4.86	−4.72	−8.78	−6.29	−5.60	−10.34
LH	−5.14	−3.94	−3.80	−7.12	−6.34	−4.92	−9.59
MHK	−4.95	−4.01	−3.87	−7.76	0.00	−4.73	−10.52
QG	0.00	−2.74	−2.60	−5.13	0.00	−2.53	−5.58
SL	−6.98	−4.68	−4.53	−9.49	−7.04	−6.76	−9.99
SP	−5.19	−4.66	−4.51	0.00	−3.02	−4.97	−9.93
WQ	−4.89	−3.56	−3.42	−6.97	−5.98	−4.67	−11.11
YF	−5.02	−4.00	−3.86	−7.97	−6.52	−4.80	−11.12
YGB	−4.97	−3.32	−3.17	−6.35	−6.91	−4.75	−10.8
QA	−7.43	−2.23	−2.09	−3.43	−6.24	−7.21	−10.19
AG	−7.05	−2.76	−2.61	−5.23	−5.43	−6.83	−9.48
CL	−5.97	−2.27	−2.12	−4.08	−6.6	−5.75	−9.62
DDS	−6.74	−3.02	−2.88	−6.16	−7.44	−6.52	−10.14
THT	−8.50	−4.55	−4.40	−8.97	−6.51	−8.28	−10.72
SG	−5.39	−1.66	−1.52	−2.85	−4.89	−5.17	−6.57
TQ	−6.55	−3.25	−3.11	−6.12	−5.24	−6.33	−11.01
JH	−7.50	−4.30	−4.16	−9.48	−5.81	−7.28	−11.48

5.4 Source of trace elements

The extent of water-rock interaction is provided with insights by trace element contents and formation processes in groundwater, which are influenced by mineral composition and rock properties (Fowler et al., 2019). The determined concentrations of 21 trace elements are summarized in Supplementary Table 3. The results of Pearson correlation analysis among all individual trace elements are shown in Figure 8.
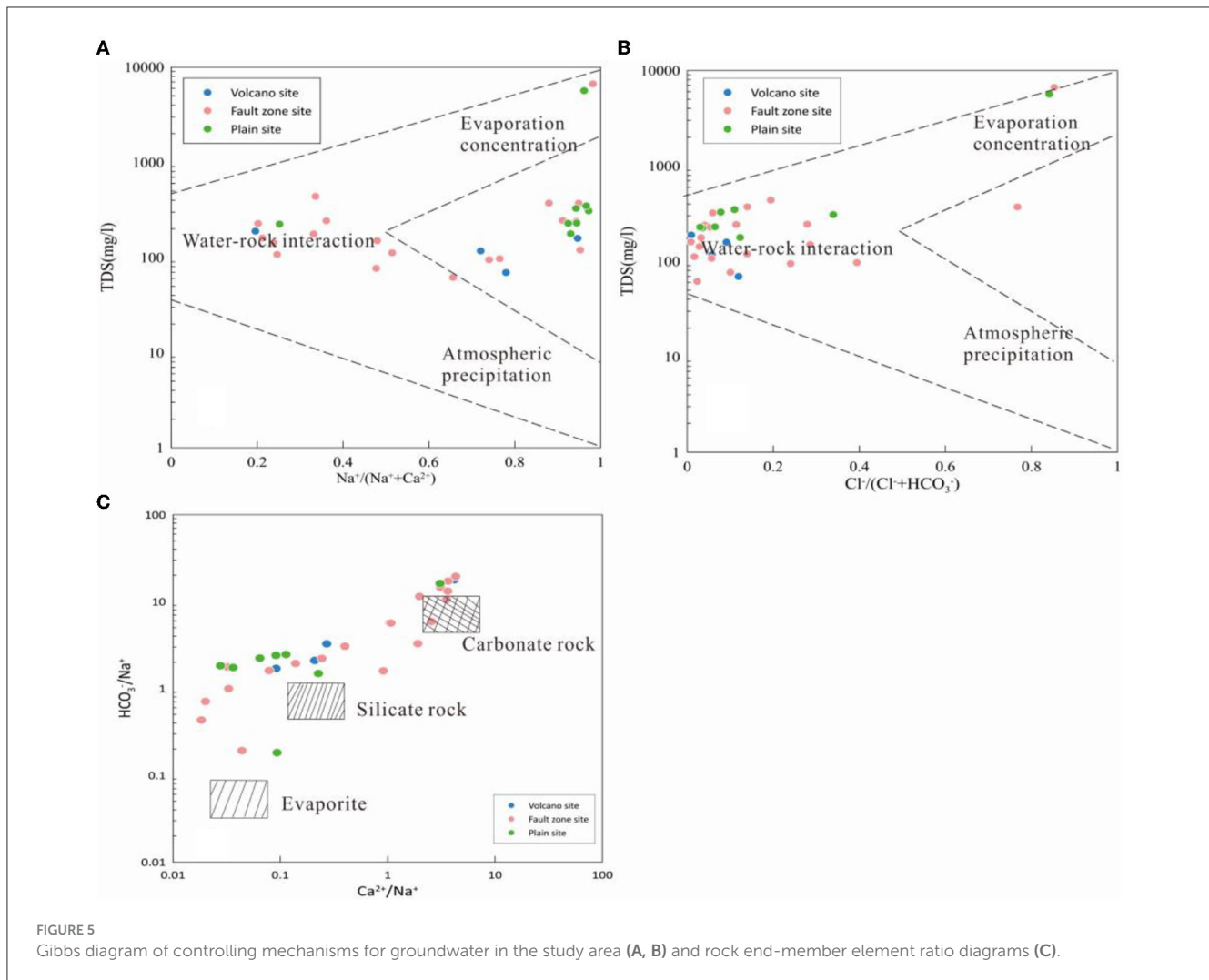
The chemical composition of groundwater is constantly influenced by water-rock interaction, evaporation and concentration, filtration and ion exchange, resulting in dynamic equilibrium (Shvartsev et al., 2018). Therefore, there is a connection between the chemical components of groundwater. Through Figure 8, the correlation degree between elements can be accurately described, and the correlation intensity between ions can be measured more accurately. As can be seen from Figure 8, in the fault zone, Li, Sr, As, B, Ba, Se, Cr, and Ti show strong correlations, while Fe, Zn, and Co are highly correlated. In the volcanic area, Li, Sr, B, Ba, Cr, Zn, Pb, and W display strong correlations, whereas Al, Mn, Fe, Ni, Cu, As, Se, Cs, Co, Rb, Mo, Ti, and Zr are strongly correlated. In the plain area, Al and Zn

FIGURE 3
Piper ternary map of Jilin groundwater sample.

FIGURE 4
Bivariate diagrams of **(A)** Ca^{2+} vs Mg^{2+}, **(B)** Ca^{2+} vs HCO_3^-, **(C)** ($Ca^{2+} + Mg^{2+}$) vs ($SO_4^{2-} + HCO_3^-$).

demonstrate strong correlations, Li, Sr, As, B, Se, Cr, and Ni show strong correlations, and Mn, Fe, Co, and Ti are highly correlated, whereas Pb, Ba, Cs, Mo, and Zr exhibit strong correlations. Due to the common occurrence of Li, Sr, As, B, and Ba in groundwater and their potential significant environmental and health implications in the groundwater cycle, such as water pollution or toxicity (Haji et al., 2021; Tong et al., 2021), the discussion will focus primarily on the sources of these five trace elements.

Sr and B replace elements in amphibole minerals in volcanic and magmatic rocks. Sr replaces Ca or K, while Ba replaces K. Sr is more mobile and therefore more abundant in water. In the lithosphere, Sr exists primarily as strontium sulfate ($SrSO_4$) and strontium carbonate ($SrCO_3$), known as lapis lazuli and strontianite respectively. During underground water flow, Sr can undergo adsorption-desorption or cation exchange on active mineral surfaces (Morales-Arredondo et al., 2022). Ba primarily

FIGURE 5
Gibbs diagram of controlling mechanisms for groundwater in the study area **(A, B)** and rock end-member element ratio diagrams **(C)**.

originates from barium-rich volcanic rocks or terrigenous marine deposits (Anadón et al., 2013). After the dissolution of barium from volcanic rock, barium and carbonate ions precipitate and bind in the formation due to limestone erosion and the presence of carbonate ions (Sun and Yao, 2005). Fixed barium carbonates can dissolve under acidic, high-temperature, high-pressure, and strong reducing conditions, leading to their abundance in water formations. There are extensive granite bodies in the fault zone, including potassium feldspar and plagioclase, while the volcanic area is mainly composed of porphyritic basalt and porphyrite, among which contain Sr and Ba rich clinopyroxene and plagioclase. In addition, there are volcanic and granite rocks deep in the plain area, which are also rich in Sr and Ba elements. Therefore, these rocks could be a potential source of trace elements Sr and Ba in the study area. Geothermal fluid upwelling commonly contains Li, B, and As as typical elements (Wang et al., 2022). Lithium silicate minerals form in volcanic and magmatic rocks, indicating deep fluid upwelling. The chemically reactive nature of lithium allows it to enter groundwater through hydrolysis (Zhang et al., 2003). The presence of B in water may originate from sediments, particularly fine particles, which make up the aquifer matrix. It may also be associated with an increase in aquifer salinity (Vinnarasi et al.,

2022). The presence of As mainly originates from the dissolution of As-rich minerals in the upper crust rocks during water-rock interaction. It is then exposed to the surface with the rise of geothermal fluids (Wang et al., 2022). Granite and metamorphic rocks exist in the fault zone, while volcanic rocks, basalt, and granitic syenite exist in the volcanic area. In the plain area, there are clinopyroxene and plagioclase. Granite, metamorphic rocks, and clinopyroxene are the main enriched rock types for Li, while volcanic rocks and basalt are rich in B and As elements. Therefore, it is possible that Li, B, and As in the study area originate from these rocks. In the study area, volcanic and metamorphic processes in the volcano region can release a substantial amount of gases and minerals into groundwater, including sulfides, carbonates, and metallic elements. The release and redistribution of these substances can alter the abundance and correlation of certain elements in groundwater, thereby impacting its water quality characteristics. Fault zones serve as pathways for hydrothermal fluids to emerge from underground, carrying rich dissolved minerals. The dissolved minerals and elements in the hydrothermal fluids further influence the correlation of elements in groundwater. Moreover, the high temperatures in the deep subsurface enhance the intensity of water-rock interactions, enabling a significant influx
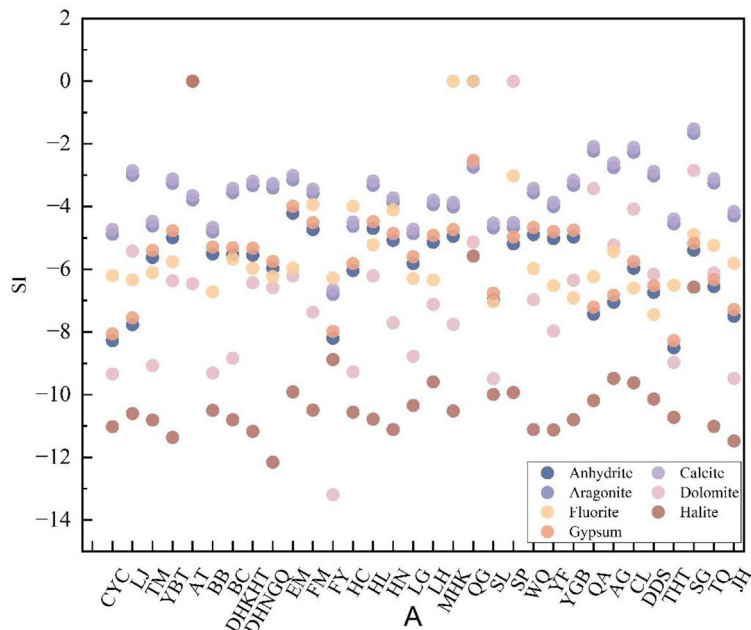
FIGURE 6
Saturation index of selected minerals in groundwater samples.
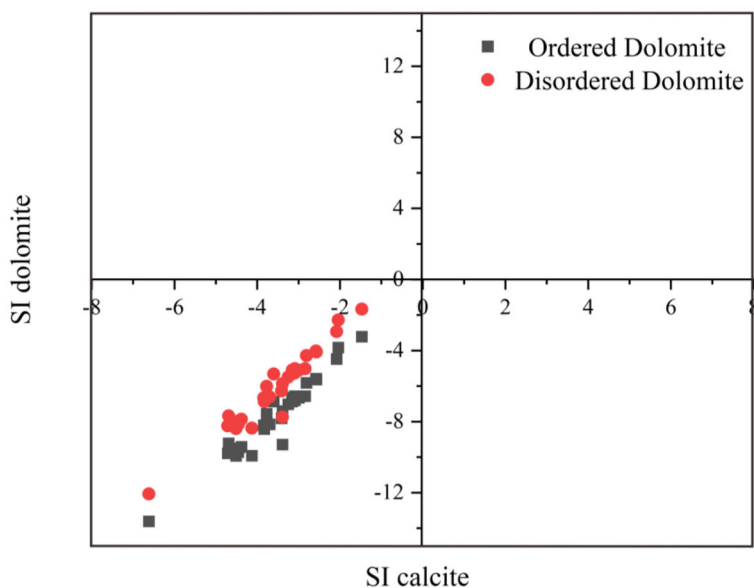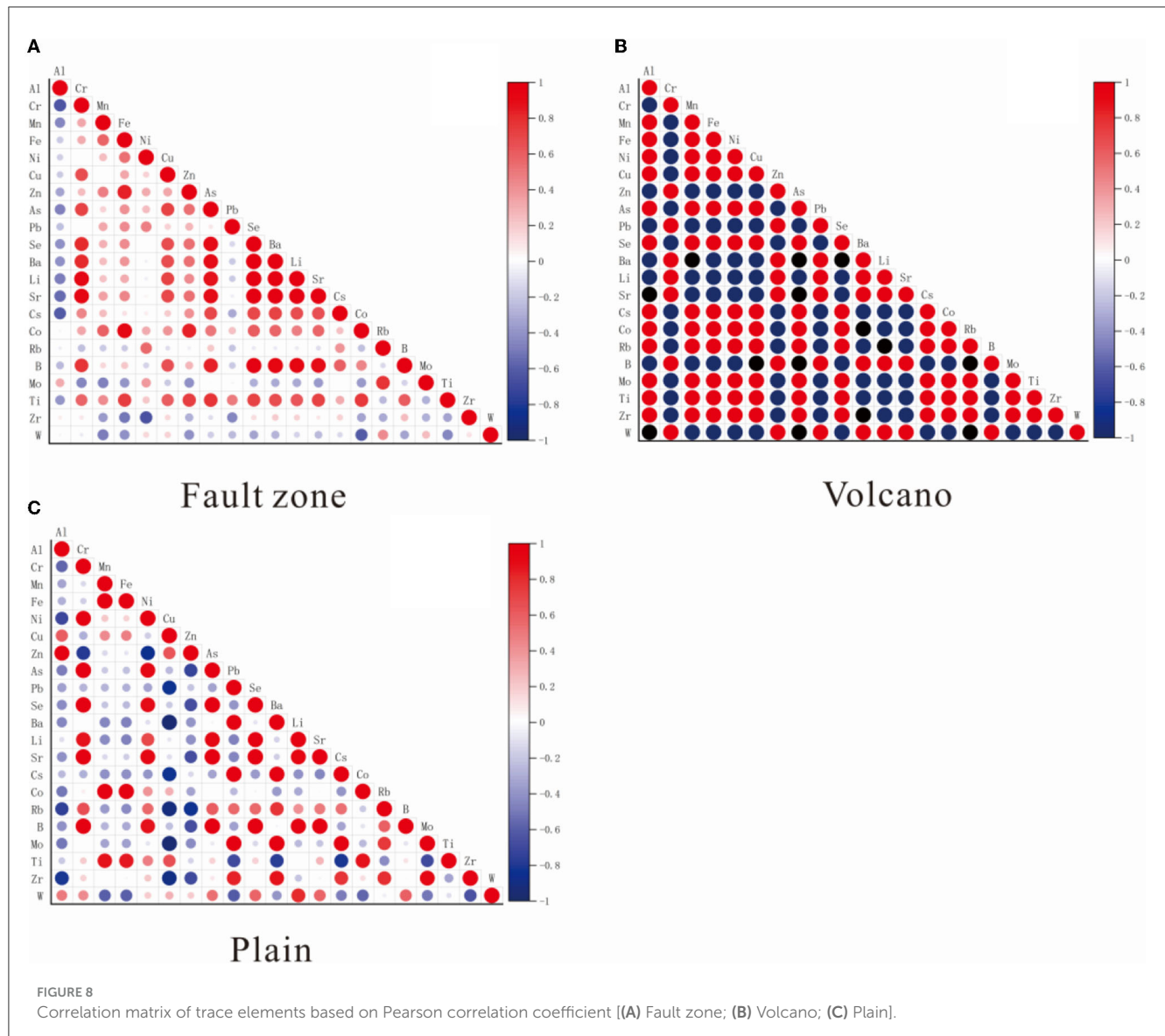

FIGURE 7
Saturation index of calcite vs. saturation indices of ordered/disordered dolomite.

of minerals from rocks into groundwater. As a result, there is a strong correlation among these five trace elements in water samples due to the reactions between groundwater and surrounding rocks during the circulation process.

5.5 Water quality evaluation

This research paper focused on the evaluation of the WQI index for 16 trace elements found in water samples, which are related to human health. Figure 9 displays the evaluation results. Most of all WQI values are below the safe level, and some elements show abnormal concentrations. Overall, the water quality falls between Category I and Category III, indicating that it is generally good. However, it can be observed that in the volcanic area, except for two points, the safety standard is somewhat exceeded by the element, while the other elements meet the Class I standard. Additionally, the majority of groundwater in the volcanic area is derived from the snow water on Changbai Mountain, which is of good quality due to the stable environment and limited human

FIGURE 8
Correlation matrix of trace elements based on Pearson correlation coefficient [**(A)** Fault zone; **(B)** Volcano; **(C)** Plain].

activities (Li et al., 2022). The elevated concentrations of Fe and Al in groundwater within the plains and fault zones may be attributed to rust and corrosion of well covers (Chen et al., 2021). Nearby industrial activities may release iron-containing wastewater and waste materials. The use of fertilizers in agricultural activities can also contribute to elevated iron levels as they may seep into the groundwater, containing iron ions (Gong et al., 2019). Additionally, the activity of the fault zone leads to an increase in the contact area between the groundwater and the underground rock, facilitating the exchange of substances between the groundwater and the fault zone, thus causing changes in dissolution, ion exchange, and chemical reactions in the groundwater. After a certain water cycle, the concentration of these elements appears to be high (Zhao et al., 2023). Based on Figure 9, it is evident that certain water samples from both the fracture area and the plain area surpass the Sr limit. The higher Sr concentration observed may be attributed to water-rock interactions with silicate and carbonate rocks in the aquifer. Sr is a bone-seeking element for humans, involved in Ca metabolism

and commonly deposited in bones, it promotes bone formation and strength (Musgrove, 2021). Consequently, the water in the study area holds significant benefits for human health.

It can be observed that the water quality is most affected in the fault zone, followed by the plain area, and least affected in the volcanic region. The phenomenon can be explained by the water flow from Changbai Mountain toward the west, passing through the fault zone, and then reaching the plain area. The possible reason behind this pattern is that although there is thermal activity in the volcanic region of Changbai Mountain, the circulation is not very strong, resulting in minimal impact. However, due to the presence of aquifers and their connectivity, this impact is transmitted to farther areas until it reaches the fault zone. In the fault zone, there is deep water circulation and intense water-rock interaction, leading to exchange of substances between groundwater and deep-seated rocks. As a result, elements get enriched in the fault zone, causing a higher degree of impact. In the plain area, although it is also affected, the circulation is
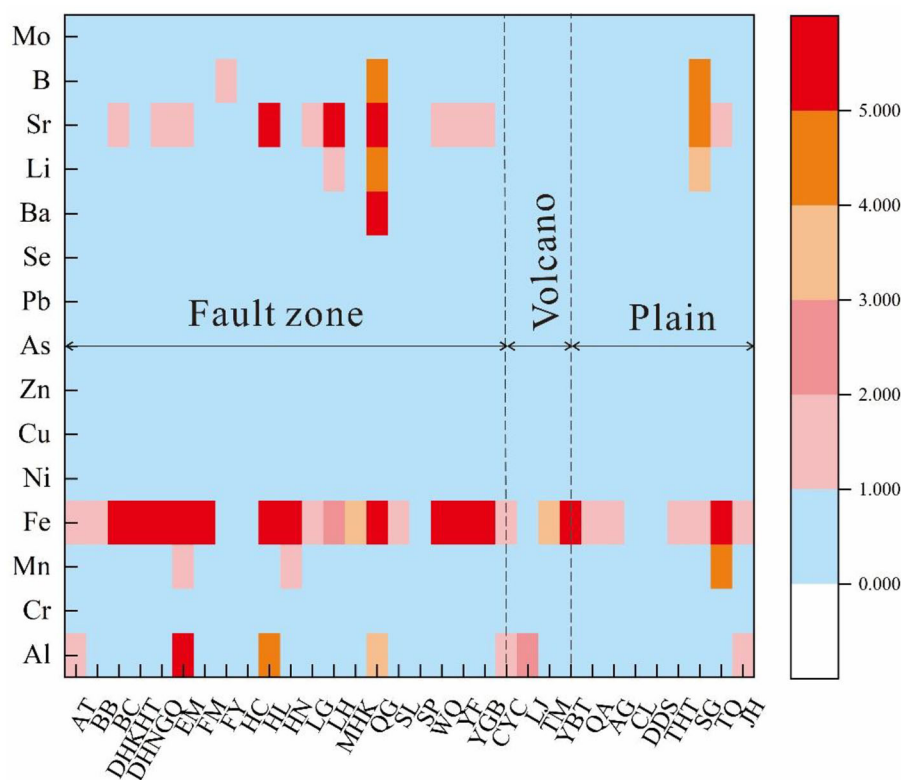
FIGURE 9
The WQI index of selected trace elements in groundwater of Jilin region.

shallow and the water-rock interaction is less intense, resulting in a relatively smaller impact.

In the fault zone and plain areas, certain individual elements exceed the permissible limits, hence necessitating the implementation of various management and protection measures. For instance, rational use of fertilizers and pesticides should be encouraged to minimize the risk of groundwater contamination. Promoting organic and ecological farming practices can also help reduce the use of chemical substances. Additionally, suitable water quality management techniques such as activated carbon adsorption and ion exchange can be employed to remove heavy metal elements from groundwater. Furthermore, it is crucial to establish a comprehensive groundwater monitoring network for regular monitoring and evaluation of water quality (Samani, 2021). Strengthening public education and raising environmental awareness are also essential in this regard.

5.6 Human health risk assessment

As depicted in Figure 10, the HQ values for HQ$_{ingestion}$, HQ$_{dermal}$, and HI values in all water samples were found to be below 1 for both children and adults. This indicates that the levels of these trace elements fall within the safe range, and adverse effects or potential non-carcinogenic risks to human health are not posed. Notably, generally higher HQ$_{ingestion}$ values than HQ$_{dermal}$ values were observed, suggesting that ingestion is the primary route of

exposure and indicating a non-carcinogenic risk within the water system. In addition, it can also be found that the HQ value of adults is higher than that of children (Table 4), indicating that the potential carcinogenic risk of adults is higher than that of children. More importantly, it can be observed that the average value of HQ in the volcanic area is generally lower than the average value in the plain and fault zone areas, indicating that the cancer risk in the volcanic area is lower than that in the other two areas. Additionally, HI values ranging from 0.1 to 1 were observed at some sites (Table 4), indicating potential long-term adverse health risks, albeit at a low non-carcinogenic risk level. Therefore, strengthening monitoring of the fault zone is crucial. Additionally, the assessment of other trace metals in the water, such as Cd, As, Cr, P, B, and Ni, should be prioritized by the local government, as these may pose higher risks to human health despite meeting drinking water standards.

5.7 Characteristics of trace elements near the fault zone

Lastly, the fault area deserves our attention. Numerous fault zones have been formed due to plate drift and compression. The YSF, which spans the southern region of Changchun, is a branch of the Tan-Lu earthquake zone (Sheng et al., 2014). This fault zone primarily consists of east-west faults, characterized by a large scale, prominent geological morphology, distinct geophysical attributes,

FIGURE 10
(a–d) Health risk index distribution maps for adults and children.
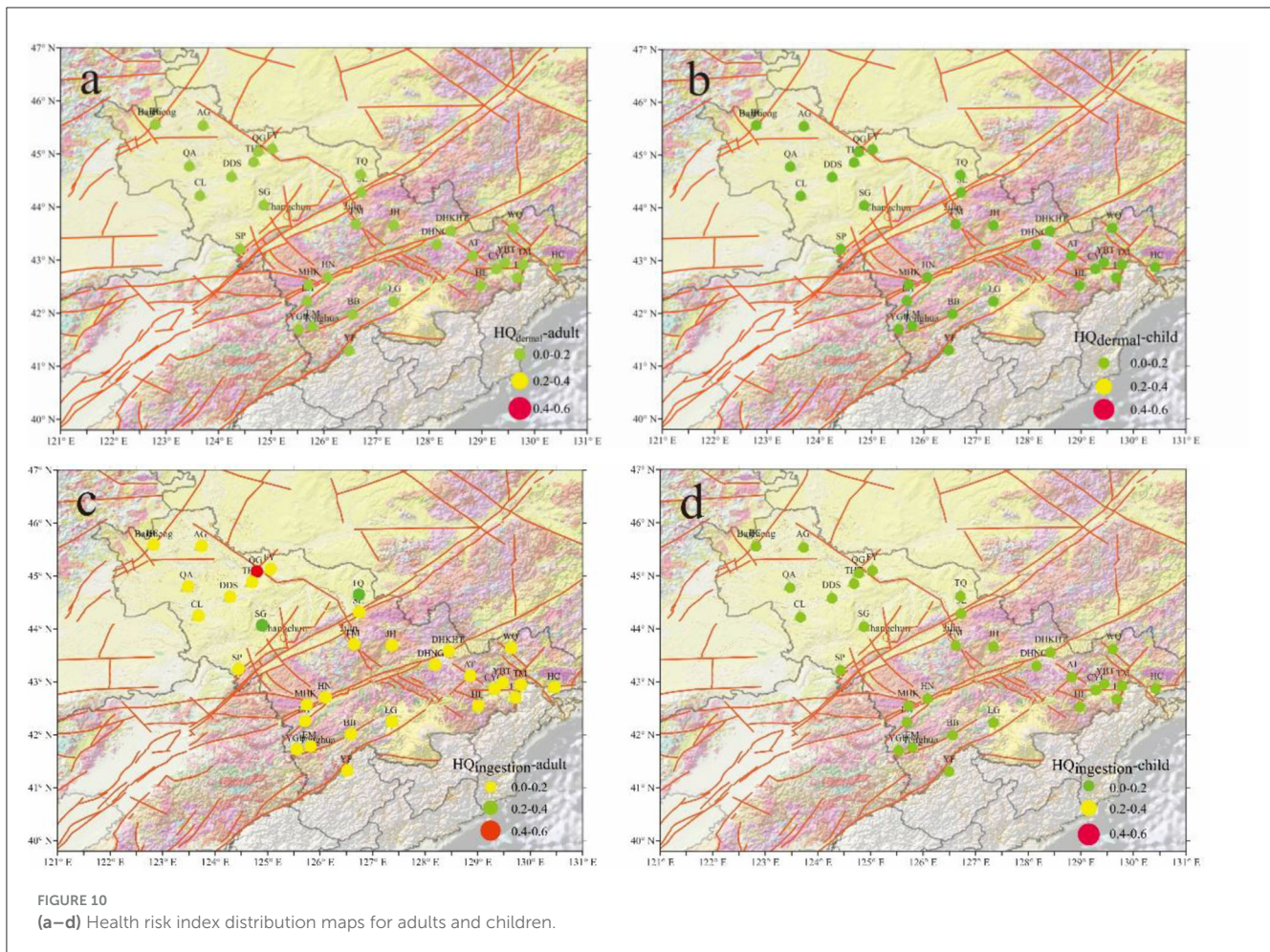
and strict control over Quaternary sedimentation. The deep trenches and fissures within these fault zones receive atmospheric precipitation and surface water.

In Figure 11, the *x*-coordinate represents groundwater locations, while the *y*-coordinate represents the concentration of elements within the water samples. It is evident that elements are enriched in BC, CL, DHKHT, EM, FM, HL, LH, QG, SG, SP, TQ, and YF. There are several causes for this enrichment:

In the Earth's crust, water and air exhibit high sensitivity to ground stress due to their inelasticity, causing them to flow from high-pressure areas to low-pressure areas. However, significant pressure drop zones are created by the extensive scale and considerable depth of active deep fault zones. Consequently, these fault zones become crucial conduits for groundwater flow and hydraulic connections between different aquifers, resulting in hydrochemical anomalies (Huang et al., 2021). Furthermore, certain cations with strong metallic properties, including Group IA and Group IIA elements in the periodic table, transition metal elements of Group VIII, and elements of Group IIIA (also known as the "boron group") such as Li, Sr, Ba, Mn, Fe, B, Al, etc., tend to concentrate within the enriched areas based on the properties of chemical elements themselves. These elements have a tendency to lose electrons due to their large ionic radius (Vlastélic et al., 2002), which makes them easily leached from

rocks and soil by water. Therefore, in the study area near the fault zone, the rocks in the Earth's crust undergo geological processes such as faulting, deformation, and fragmentation. These geological processes cause the fractures in the vicinity of the fault zone, creating more fissures and pore spaces. These fractured zones and fissures serve as pathways for groundwater flow, allowing contact between groundwater and trace elements in the rocks, gradually leading to enrichment. During the process of groundwater flow, it rapidly transports through the fractured zones and fissures surrounding the fault zone. This fast water flow carries away trace elements from the rocks, making them more easily absorbed and enriched by groundwater. Additionally, the fault zone may involve uplift or subsidence of groundwater layers, which also contributes to the accumulation of trace elements in groundwater within that area. Interestingly, this conclusion is consistent with the findings in Section 5.5 as well.

5.8 Groundwater circulation model in Jilin

Understanding the origin and transport pathways of groundwater in the study area is crucial for studying the hydrological properties of the groundwater system. Based on previous studies and the findings of this study, we have established

TABLE 4 List of human health risk assessment.

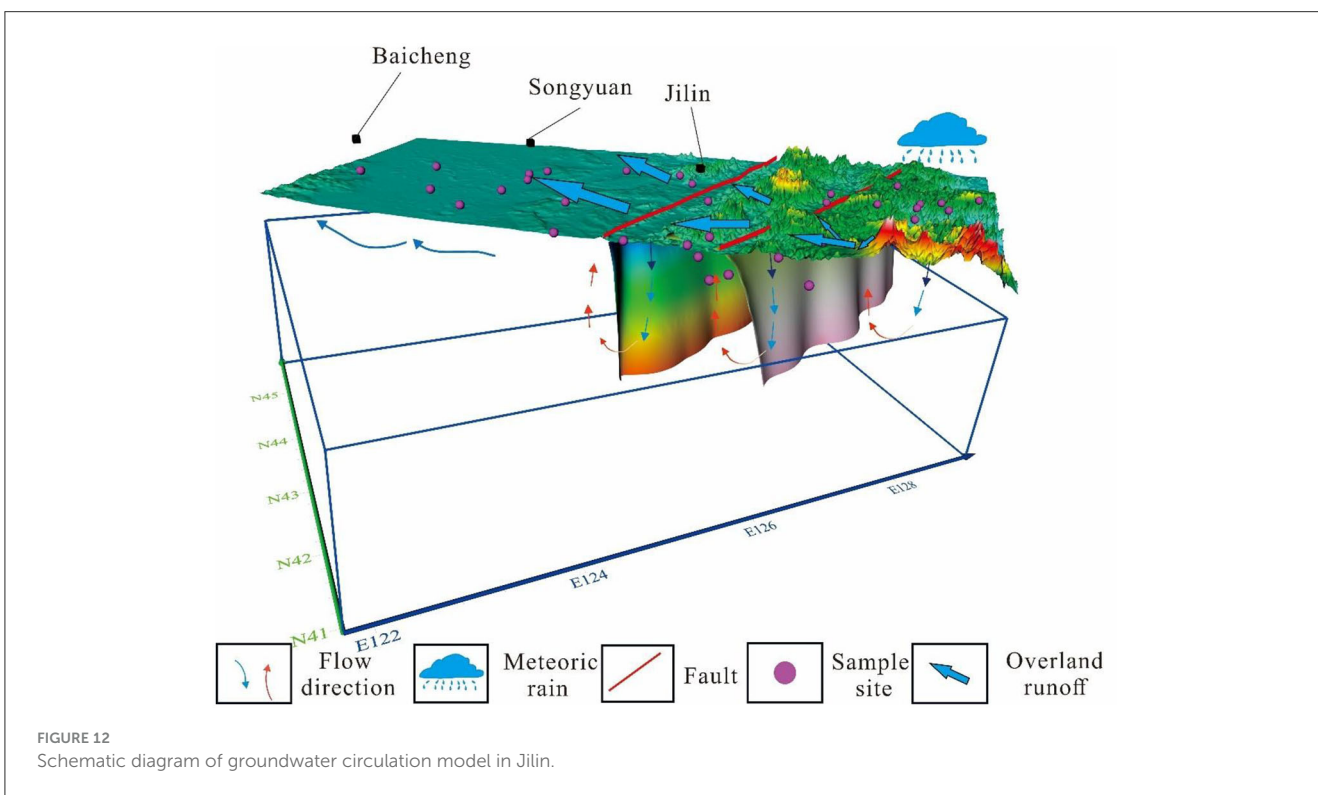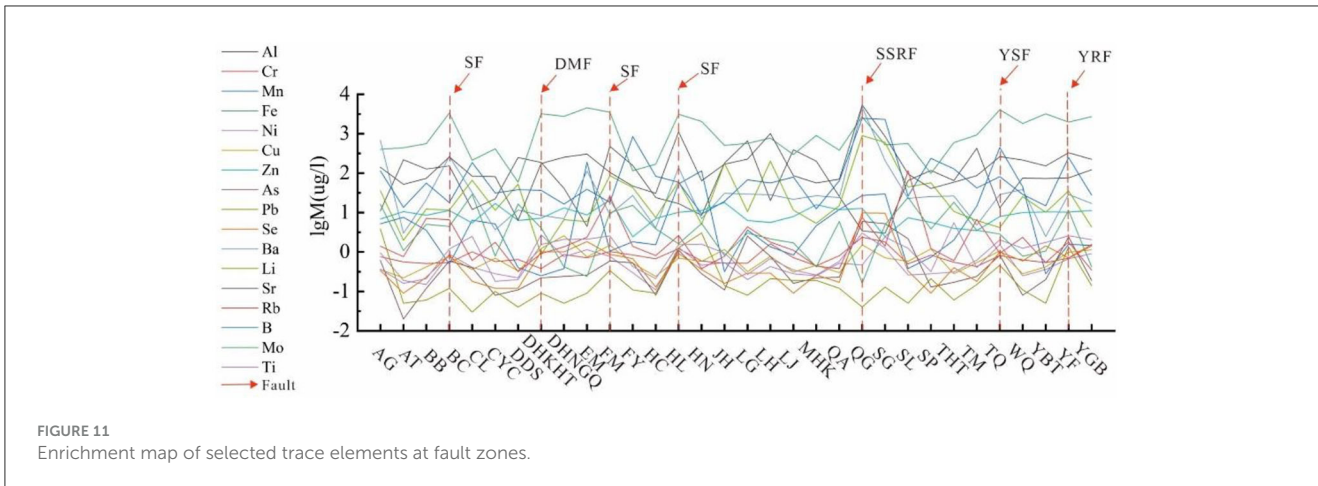|	HQ$_{ingestion}$-adult	HQ$_{dermal}$-adult	HQ$_{ingestion}$-child	HQ$_{dermal}$-child
AT	0.025	0.002	0.015	0.005
BB	0.027	0.002	0.012	0.003
BC	0.109	0.004	0.039	0.004
DHKHT	0.081	0.002	0.035	0.005
DHNGQ	0.067	0.003	0.023	0.001
EM	0.200	0.016	0.062	0.001
FM	0.117	0.004	0.052	0.012
FY	0.037	0.002	0.017	0.004
HC	0.013	0.001	0.005	0.001
HL	0.153	0.008	0.048	0.001
HN	0.134	0.009	0.041	0.001
LG	0.136	0.003	0.063	0.017
LH	0.057	0.003	0.018	0.001
MHK	0.040	0.002	0.019	0.005
QG	0.588	0.029	0.177	0.002
SL	0.104	0.002	0.035	0.002
SP	0.020	0.002	0.010	0.003
WQ	0.068	0.005	0.023	0.002
YF	0.151	0.003	0.049	0.002
YGB	0.076	0.004	0.028	0.003
CYC	0.023	0.002	0.008	0.001
LJ	0.032	0.002	0.023	0.010
TM	0.051	0.002	0.030	0.011
YBT	0.072	0.002	0.024	0.002
QA	0.032	0.002	0.011	0.001
AG	0.113	0.005	0.036	0.001
CL	0.030	0.002	0.010	0
DDS	0.043	0.003	0.026	0.009
THT	0.035	0.002	0.022	0.002
SG	0.256	0.007	0.080	0.001
TQ	0.337	0.032	0.104	0.001
JH	0.027	0.001	0.015	0.004

a conceptual model for the genesis and hydrological cycle of groundwater in the Jilin region. As depicted in Figure 12, it is evident that the primary recharge source in the study area is atmospheric precipitation. Surface runoff flows from the eastern volcanic region to the western fault zone and plain area. Groundwater circulation is more extensive in the fault zone, while it remains relatively shallow in the plain area. Although the volcanic region exhibits hydrothermal activities, the groundwater circulation is not particularly intense. During the circulation process, groundwater undergoes water-rock interactions, thereby

carrying abundant geochemical information. 'Furthermore, the results of the study indicate that faults play a significant role in controlling the movement of crustal fluids. By gaining a comprehensive understanding of the origin and transport pathways of groundwater in the study area, we can better grasp the hydrological characteristics of the groundwater system and provide valuable insights for further research in related fields.

6 Conclusion

In this study, the authors conducted an investigation on the geochemical properties of 32 groundwater samples collected from Jilin Province. Additionally, they performed an environmental assessment on these samples. The conclusions are as follows:

(1) The hydrogen and oxygen isotopes analysis of atmospheric precipitation in Jilin Province indicates that the primary source of groundwater in the study area is atmospheric precipitation. This, combined with the replenishment elevation range of groundwater (1,430–2,348 m). Moreover, it is important to note that the chemical composition of water generally varies depending on the geographical region. In plain areas, water is predominantly characterized by Na-HCO$_3$ composition, while in volcanic regions, it tends to exhibit Ca·Na-HCO$_3$ composition. In fault zones, the dominant composition is Ca-HCO$_3$. The main ion composition of groundwater is primarily controlled by the weathering of rocks, with carbonate rocks and silicate rocks having a greater influence on groundwater composition and evaporite rocks having a lesser influence. These variations in chemical composition further underscore the regional differences in water characteristics within the study area.

(2) In the study area, the water flow originates from the Changbai Mountain volcanic region and moves westward toward the fault zone and plain areas. The volcanic region exhibits a strong correlation between trace elements in groundwater due to the presence of hydrothermal activity. However, the circulation of groundwater in this region is not very intense, resulting in relatively good water quality with minimal impact. On the other hand, the fault zone, being located in a fault belt, experiences deep circulation, leading to a more pronounced interaction between groundwater and rock formations. This intense interaction contributes to a strong correlation between trace elements in groundwater. While the water quality generally meets requirements, it is significantly affected, resulting in the enrichment of trace elements in this area. In the plain areas, the shallow circulation of groundwater results in a relatively weaker correlation between trace elements compared to the volcanic region and fault zone. The water quality in this region falls between that of the volcanic region and fault zone, generally considered good with minor impact. Overall, the geochemical characteristics of trace elements in groundwater are influenced by the geological environment. Different regions exhibit variations in the content and correlation of trace elements in groundwater. Understanding these

FIGURE 11
Enrichment map of selected trace elements at fault zones.

FIGURE 12
Schematic diagram of groundwater circulation model in Jilin.

characteristics is crucial for the management and protection of groundwater resources.

(3) According to the results of water quality evaluation and human health risk assessment, the water quality in the research area is good, indicating that the damage and pollution of groundwater are relatively low. This evaluation result indicates that the research area has good sustainability of groundwater compared to the announcement issued by the Jilin Provincial Department of Water Resources. In Jilin Province, a series of ecological and environmental issues such as continuous groundwater decline, aquifer depletion, and land subsidence have hindered sustainable economic and social development. Therefore, to maintain the groundwater resources in the

research area, it is necessary to strengthen groundwater management and protection efforts. In addition, it is vital to develop a robust groundwater monitoring system that can routinely monitor and assess water quality comprehensively. It is equally important to enhance public education and raise awareness of environmental issues related to groundwater protection.

Data availability statement

The original contributions presented in the study are included in the article/Supplementary material, further inquiries can be directed to the corresponding authors.

Author contributions

ZZe: Conceptualization, Investigation, Software, Writing – original draft. YC: Conceptualization, Data curation, Software, Writing – review & editing. XZ: Conceptualization, Funding acquisition, Software, Validation, Writing – review & editing. XP: Conceptualization, Software, Methodology, Writing – review & editing. FS: Conceptualization, Investigation, Software, Writing – review & editing. YL: Conceptualization, Investigation, Software, Writing – review & editing. JT: Conceptualization, Methodology, Software, Writing – review & editing. MH: Conceptualization, Methodology, Supervision, Writing – review & editing. YZ: Conceptualization, Methodology, Software, Writing – review & editing. YY: Conceptualization, Investigation, Software, Writing – review & editing. ZZo: Conceptualization, Investigation, Software, Writing – review & editing. YW: Conceptualization, Investigation, Software, Writing – review & editing. BY: Conceptualization, Methodology, Software, Writing – review & editing. GX: Conceptualization, Investigation, Software, Writing – review & editing. SC: Conceptualization, Investigation, Software, Writing – review & editing.

Funding

Conflict of interest

The authors declare that the research was conducted in the absence of any commercial or financial relationships that could be construed as a potential conflict of interest.

Publisher's note

All claims expressed in this article are solely those of the authors and do not necessarily represent those of their affiliated organizations, or those of the publisher, the editors and the reviewers. Any product that may be evaluated in this article, or claim that may be made by its manufacturer, is not guaranteed or endorsed by the publisher.

Supplementary material

The Supplementary Material for this article can be found online at: https://www.frontiersin.org/articles/10.3389/frwa.2023. 1315805/full#supplementary-material

References

Adelodun, B., Ajibade, F. O., Ighalo, J. O., Odey, G., Ibrahim, R. G., Kareem, K. Y., et al. (2021). Assessment of socioeconomic inequality based on virus-contaminated water usage in developing countries: a review. *Environ. Res.* 192, 110309. doi: 10.1016/j.envres.2020.110309

Adeyeye, O. A., Xiao, C., Zhang, Z., Yawe, A. S., and Liang, X. (2021). Groundwater fluoride chemistry and health risk assessment of multi-aquifers in Jilin Qianan, Northeastern China. *Ecotoxicol. Environ. Saf.* 211, 111926. doi: 10.1016/j.ecoenv.2021.111926

Adimalla, N., and Qian, H. (2019). Groundwater quality evaluation using water quality index (WQI) for drinking purposes and human health risk (HHR) assessment in an agricultural region of Nanganur, south India. *Ecotoxicol. Environ. Saf.* 176, 153–161. doi: 10.1016/j.ecoenv.2019.03.066

Adimalla, N., and Taloor, A. K. (2020). Hydrogeochemical investigation of groundwater quality in the hard rock terrain of South India using Geographic Information System (GIS) and groundwater quality index (GWQI) techniques. *Groundw. Sustain. Dev.* 10, 100288. doi: 10.1016/j.gsd.2019.100288

Aithani, D., Jyethi, D. S., Siddiqui, Z., Yadav, A. K., and Khillare, P. S. (2020). Source apportionment, pollution assessment, and ecological and human health risk assessment due to trace metals contaminated groundwater along urban river floodplain. *Groundw. Sustain. Dev.* 11, 100445. doi: 10.1016/j.gsd.2020.100445

Al-Gburi, H. F., and Al-Tawash, B. S. Al–Tamimi, O. S., Schüth, C. (2022). Stable isotope composition in precipitation and groundwater of Shwan Sub-Basin, Kirkuk governorate, northeast of Iraq. *Water Sci. Technol. Water Supply* 22, 7442–7459. doi: 10.2166/ws.2022.327

An, R., Li, B., Zhong, S., Peng, G., Li, J., Ma, R., et al. (2023). Distribution, source identification, and health risk of emerging organic contaminants in groundwater of Xiong'an New Area, Northern China. *Sci. Total Environ.* 893, 164786. doi: 10.1016/j.scitotenv.2023.164786

Anadón, P., Canet, C., and Friedrich, W. L. (2013). Aragonite stromatolitic buildups from Santorini (Aegean Sea, Greece): geochemical and palaeontological constraints of the caldera palaeoenvironment prior to the Minoan eruption (ca3600yrbp). *Sedimentology* 60, 1128–1155. doi: 10.1111/sed.12025

Apollaro, C., Caracausi, A., Paternoster, M., Randazzo, P., Aiuppa, A., De Rosa, R., et al. (2020). Fluid geochemistry in a low-enthalpy geothermal field along a sector of southern Apennines chain (Italy). *J. Geochem. Explor.* 219, 106618. doi: 10.1016/j.gexplo.2020.106618

Bian, J., Sun, W., Li, J., Li, Y., Ma, Y., Li, Y., et al. (2023). Hydrochemical formation mechanism of mineral springs in Changbai Mountain (China). *Environ. Earth Sci.* 82, 145. doi: 10.1007/s12665-023-10795-5

Bianchini, G., Pennisi, M., Cioni, R., Muti, A., Cerbai, N., Kloppmann, W., et al. (2005). Hydrochemistry of the high-boron groundwaters of the Cornia aquifer (Tuscany, Italy). *Geothermics* 34, 297–319. doi: 10.1016/j.geothermics.2005.04.002

Bodrud-Doza, M., Islam, S. M. D.-U., Hasan, M. T., Alam, F., Haque, M. M., Rakib, M. A., et al. (2019). Groundwater pollution by trace metals and human health risk assessment in central west part of Bangladesh. *Groundw. Sustain. Dev.* 9, 100219. doi: 10.1016/j.gsd.2019.100219

Cai, W., Li, X., Zhang, M., and Zhang, B. (2003). A study on the hydrogeology and environmental geology of Jilin Province. [In Chinese]. *Jilin Geol.* 22, 52–57.

Chai, Y., Xiao, C., Li, M., and Liang, X. (2020). Hydrogeochemical characteristics and groundwater quality evaluation based on multivariate statistical analysis. *Water* 12, 2792. doi: 10.3390/w12102792

Chen, Y., Zhang, Y., He, J., Zhang, J., Lang, Q., Liu, H., et al. (2021). Assessment of groundwater quality and pollution in the songnen Plain of Jilin Province, Northeast China. *Water* 13, 2414. doi: 10.3390/w13172414

Craig, H. (1961). Isotopic variations in meteoric *Waters Sci.* 133, 1702–1703. doi: 10.1126/science.133.3465.1702

Dash, C. J., Sarangi, A., Singh, D. K., Adhikary, P. P. (2019). Numerical simulation to assess potential groundwater recharge and net groundwater use in a semi-arid region. *Environ. Monit. Assess.* 191, 371. doi: 10.1007/s10661-019-7508-y

Deshaee, A., Shakeri, A., Taran, Y., Mehrabi, B., Farhadian, M., Zelenski, M., et al. (2020). Geochemistry of bazman thermal springs, southeast Iran. *J. Volcanol. Geotherm. Res.* 390, 106676. doi: 10.1016/j.jvolgeores.2019.106676

Fang, Z., Ding, X., and Gao, H. (2022). Local-scale groundwater sustainability assessment based on the response to groundwater mining (MGSI): a case study of Da'an City, Jilin Province, China. *Sustainability* 14, 5618. doi: 10.3390/su14095618

Farhadkhani, M., Nikaeen, M., Yadegarfar, G., Hatamzadeh, M., Pourmohammadbagher, H., Sahbaei, Z., et al. (2018). Effects of irrigation with secondary treated wastewater on physicochemical and microbial properties of soil and produce safety in a semi-arid area. *Water Res.* 144, 356–364. doi: 10.1016/j.watres.2018.07.047

Feng, M., Zhang, W., Zhang, S., Sun, Z., Li, Y., Huang, Y., et al. (2022). The role of snowmelt discharge to runoff of an alpine watershed: evidence from water stable isotopes. *J. Hydrol.* 604, 127209. doi: 10.1016/j.jhydrol.2021.127209

Fowler, A. P. G., Zierenberg, R. A., Reed, M. H., Palandri, J., Óskarsson, F., Gunnarsson, I., et al. (2019). Rare earth element systematics in boiled fluids from basalt-hosted geothermal systems. *Geochim. Cosmochim. Acta* 244, 129–154. doi: 10.1016/j.gca.2018.10.001

Gao, B., Gao, L., Gao, J., Xu, D., Wang, Q., Sun, K., et al. (2019). Simultaneous evaluations of occurrence and probabilistic human health risk associated with trace elements in typical drinking water sources from major river basins in China. *Sci. Total Environ.* 666, 139–146. doi: 10.1016/j.scitotenv.2019.02.148

Giggenbach, W. F. (1988). Geothermal solute equilibria. Derivation of Na-K-Mg-Ca geoindicators. *Geochim. Cosmochim. Acta* 52, 2749–2765. doi: 10.1016/0016-7037(88)90143-3

Githaiga, K. B., Njuguna, S. M., Gituru, R. W., and Yan, X. (2021). Water quality assessment, multivariate analysis and human health risks of heavy metals in eight major lakes in Kenya. *J. Environ. Manage.* 297, 113410. doi: 10.1016/j.jenvman.2021.113410

Gong, X., Bian, J., Wang, Y., Jia, Z., and Wan, H. (2019). Evaluating and predicting the effects of land use changes on water quality using SWAT and CA–Markov models. *Water Resour. Manag.* 33, 4923–4938. doi: 10.1007/s11269-019-02427-0

Gu, Z., Bian, J., Wu, J., Ruan, D., Yu, Y., Zhang, H., et al. (2022). Effects of anthropogenic activities on hydrochemical characteristics of ground water of Da'an irrigation area in Western of Jilin Province. *Environ. Sci. Pollut. Res.* 29, 20479–20495. doi: 10.1007/s11356-021-16937-1

Guo, J., Zhou, X., Wang, L., Zhang, Y., Shen, X., Zhou, H., et al. (2018). Hydrogeochemical characteristics and sources of salinity of the springs near Wenquanzhen in the eastern Sichuan Basin, China. *Hydrogeol. J.* 26, 1137–1151. doi: 10.1007/s10040-017-1692-z

Guo, S., Chen, R., and Li, H. (2022). Surface sublimation/evaporation and condensation/deposition and their links to westerlies during 2020 on the August-One Glacier, the semi-arid Qilian Mountains of Northeast Tibetan Plateau. *J. Geophys. Res.* 127. doi: 10.1029/2022JD036494

Haji, M., Karuppannan, S., Qin, D., Shube, H., and Kawo, N. S. (2021). Potential human health risks due to groundwater fluoride contamination: a case study using multi-techniques approaches (GWQI, FPI, GIS, HHRA) in Bilate River Basin of Southern Main Ethiopian Rift, Ethiopia. *Arch. Environ. Contam. Toxicol.* 80, 277–293. doi: 10.1007/s00244-020-00802-2

Hao, Q., Li, Y., Xiao, Y., Yang, H., Zhang, Y., Wang, L., et al. (2023). Hydrogeochemical fingerprint, driving forces and spatial availability of groundwater in a coastal plain, Southeast China. *Urban Clim.* 51, 101611. doi: 10.1016/j.uclim.2023.101611

Heiß, L., Bouchaou, L., Tadoumant, S., and Reichert, B. (2020). Multi-tracer approach for assessing complex aquifer systems under arid climate: case study of the River Tata catchment in the Moroccan Anti-Atlas Mountains. *Appl. Geochem.* 120, 104671. doi: 10.1016/j.apgeochem.2020.104671

Huan, H., Zhang, B.-T., Kong, H., Li, M., Wang, W., Xi, B., et al. (2018). Comprehensive assessment of groundwater pollution risk based on HVF model: a case study in Jilin City of northeast China. *Sci. Total Environ.* 628–629, 1518–1530. doi: 10.1016/j.scitotenv.2018.02.130

Huang, J., He, H., Tan, W., Liang, X., Ma, L., Wang, Y., et al. (2021). Groundwater controls REE mineralisation in the regolith of South China. *Chem. Geol.* 577, 120295. doi: 10.1016/j.chemgeo.2021.120295

Jilin Provincial Environmental Protection Bureau (2022). report on the ecological environment status in Jilin Province in 2022. *Environ. Sci. J.* 10, 23–29.

Kawo, N. S., and Karuppannan, S. (2018). Groundwater quality assessment using water quality index and GIS technique in Modjo River Basin, central Ethiopia. *J. African Earth Sci.* 147, 300–311. doi: 10.1016/j.jafrearsci.2018.06.034

Khaliq, M. A., Javed, M. T., Hussain, S., Imran, M., Mubeen, M., Nasim, W., et al. (2022). Assessment of heavy metal accumulation and health risks in okra (*Abelmoschus esculentus* L.) and spinach (*Spinacia oleracea* L.) fertigated with wastwater. *Int. J. Food Microbiol.* 9, 11. doi: 10.1186/s40550-022-00097-2

Lei, Y., Zhao, Z., Zhang, B., Tang, X., Luo, Y., Wang, G., et al. (2022). genesis of significance of carbonated thermal water springs in Xining Basin, China. *Water* 14, 4058. doi: 10.3390/w14244058

Li, Y., Bian, J., Li, J., Ma, Y., and Anguiano, J. H. H. (2022). Hydrochemistry and stable isotope indication of natural mineral water in Changbai Mountain, China. *J. Hydrol. Reg. Stud.* 40, 101047. doi: 10.1016/j.ejrh.2022.101047

Li, Z., Fu, Z., Wang, S., Zhang, Y., Zhang, J., Liu, Y., et al. (2023). Spatial distribution, ecological risk, and human health assessment of heavy metals in lake surface sections—a case study of Qinghai Lake, China. *Environ. Sci. Pollut. Res.* 30, 5137–5149. doi: 10.1007/s11356-022-22293-5

Li, Z., Yang, Q., Yang, Y., Xie, C., and Ma, H. (2020). Hydrogeochemical controls on arsenic contamination potential and health threat in an intensive agricultural area, northern China. *Environ. Pollut.* 256, 113455. doi: 10.1016/j.envpol.2019.113455

Liu, J., Deng, X., Hou, M., Wang, X., Shi, Z., Ni, S., et al. (2022). Thermodynamic control on chemical weathering of river bedrock at the Aba and Qamdo in Kaschin-beck disease region, eastern Tibet Plateau. *Geo. Geoenviron.* 100126. doi: 10.1016/j.geogeo.2022.100126

Liu, J., Li, L., Ren, C., Wang, Z., and Zhang, B. (2017). GIS-based division of shallow groundwater function in Jilin Province. [In Chinese]. *J. Arid Environ.* 31, 166–171. doi: 10.13448/j.cnki.jalre.2017.397

Liu, J., Liu, E., and Zhao Y. (1997). Discussion on the stable isotope time-space distribution law of China atmospheric precipitation. *SI Sci. Technol.* 3, 34–39.

Liu, J., Peng, Y., Li, C., Gao, Z., and Chen, S. (2021). An investigation into the hydrochemistry, quality and risk to human health of groundwater in the central region of Shandong Province, North China. *J. Clean. Prod.* 282, 125416. doi: 10.1016/j.jclepro.2020.125416

Maliva, R. G. (2020). "Anthropogenic aquifer recharge and water quality," in *Anthropogenic Aquifer Recharge*, ed. R. G. Maliva (Berlin: Springer Int Publ), 133–164. doi: 10.1007/978-3-030-11084-0

Morales-Arredondo, J. I., Armienta Hernández, M. A., Cuellar-Ramírez, E., Morton-Bermea, O., and Ortega-Gutiérrez, J. E. (2022). Hydrogeochemical behavior of Ba, B, Rb, and Sr in an urban aquifer located in central Mexico and its environmental implications. *J. S. Am. Earth Sci.* 116, 103870. doi: 10.1016/j.jsames.2022.103870

Musgrove, M. (2021). The occurrence and distribution of strontium in U.S. groundwater. *Appl. Geochem.* 126, 104867. doi: 10.1016/j.apgeochem.2020.104867

Nadikatla, S. K., Mushini, V. S., and Mudumba, P. S. M. K. (2020). Water quality index method in assessing groundwater quality of Palakonda mandal in Srikakulam district, Andhra Pradesh, India. *Appl. Water Sci.* 10, 30. doi: 10.1007/s13201-019-1110-x

Ndoye, S., Diedhiou, M., Celle, H., Faye, S., Baalousha, M., Le Coustumer, P., et al. (2023). Hydrogeochemical characterization of groundwater in a coastal area, central western Senegal. *Front. Water* 4, 1097396. doi: 10.3389/frwa.2022.1097396

Ndoye, S., Fontaine, C., Gaye, C., and Razack, M. (2018). Groundwater quality and suitability for different uses in the saloum area of Senegal. *Water* 10, 1837. doi: 10.3390/w10121837

Panneerselvam, B., Muniraj, K., Duraisamy, K., Pande, C., Karuppannan, S., Thomas, M., et al. (2023). An integrated approach to explore the suitability of nitrate-contaminated groundwater for drinking purposes in a semiarid region of India. *Environ. Geochem. Health* 45, 647–663. doi: 10.1007/s10653-022-01237-5

Qi, Y., and Tong, P. (2023). Structure of the crustal magmatic system in the geysers-clear lake area (Northern California) imaged by adjoint-state travel-time tomography. *Seismol. Res. Lett.* 94, 414–427. doi: 10.1785/0220220131

Qiao, D., Zhou, J., Liang, S., and Fu, X. (2019). Combined effects of precipitation and temperature on the responses of forest spring phenology to winter snow cover dynamics in Northeast China. *IEEE Access* 7, 138950–138962. doi: 10.1109/ACCESS.2019.2943202

Qiu, H., Gui, H., Xu, H., Cui, L., and Yu, H. (2023). Occurrence, controlling factors and noncarcinogenic risk assessment based on Monte Carlo simulation of fluoride in mid-layer groundwater of Huaibei mining area, North China. *Sci. Total Environ.* 856, 159112. doi: 10.1016/j.scitotenv.2022.159112

Qiu, S., Liang, X., Xiao, C., Huang, H., Fang, Z., Lv, F., et al. (2015). Numerical simulation of groundwater flow in a River Valley Basin in Jilin Urban Area, China. *Water* 7, 5768–5787. doi: 10.3390/w7105768

Qu, B., Zhang, Y., Kang, S., and Sillanpää, M. (2019). Water quality in the tibetan plateau: major ions and trace elements in rivers of the "Water Tower of Asia". *Sci. Total Environ.* 649, 571–581. doi: 10.1016/j.scitotenv.2018.08.316

Ren, W., Yao, T., and Xie, S. (2018). Stable isotopic composition reveals the spatial and temporal dynamics of discharge in the large river of Yarlungzangbo in the Tibetan Plateau. *Sci. Total Environ.* 625, 373–381. doi: 10.1016/j.scitotenv.2017.12.310

Samani, S. (2021). Assessment of groundwater sustainability and management plan formulations through the integration of hydrogeological, environmental, social, economic and policy indices. *Groundw. Sustain. Dev.* 15, 100681. doi: 10.1016/j.gsd.2021.100681

Sheng, J., Yu, G. Y., Wang, Y. M., and Lv, H. (2014). Application of polarization remote sensing to identify activity of Yitong-Shulan Fault, Jilin Province, China. *Adv. Mat. Res.* 1065–1069, 2246–2250. doi: 10.4028/www.scientific.net/AMR.1065-1069.2246

Shvartsev, S. L., Sun, Z., Borzenko, S. V., Gao, B., Tokarenko, O. G., Zippa, E. V., et al. (2018). Geochemistry of the thermal waters in Jiangxi Province, China. *Appl. Geochem.* 96, 113–130. doi: 10.1016/j.apgeochem.2018.06.010

Soujanya Kamble, B., Saxena, P. R., Kurakalva, R. M., and Shankar, K. (2020). Evaluation of seasonal and temporal variations of groundwater quality around Jawaharnagar municipal solid waste dumpsite of Hyderabad city, India. *SN Appl. Sci.* 2, 498. doi: 10.1007/s42452-020-2199-0

Strohmenger, L., Ackerer, P., Belfort, B., and Pierret, M. C. (2022). Local and seasonal climate change and its influence on the hydrological cycle in a mountainous forested catchment. *J. Hydrol.* 610, 127914. doi: 10.1016/j.jhydrol.2022.127914

Su, B., Xiao, C., Chen, D., Huang, Y., Che, Y., Zhao, H., et al. (2022). Glacier change in China over past decades: Spatiotemporal patterns and influencing factors. *Earth Sci. Rev.* 226, 103926. doi: 10.1016/j.earscirev.2022.103926

Sun, X., and Yao, H. (2005). Geochemical characteristics and genesis of Yingxi barite deposits in Hunan Province. *Xinjiang Geol.* 23, 5.

Tong, S., Li, H., Tudi, M., Yuan, X., and Yang, L. (2021). Comparison of characteristics, water quality and health risk assessment of trace elements in surface water and groundwater in China. *Ecotoxicol. Environ. Saf.* 219, 112283. doi: 10.1016/j.ecoenv.2021.112283

US EPA (2004). *Risk Assessment Guidance for Superfund Volume I: Human Health Evaluation Manual (Part E, Supplemental Guidance for Dermal Risk Assessment) Final.* Washington, DC: Office of Superfund Remediation and Technology Innovation U.S. Environmental Protection Agency.

Ustaoglu, F., Tepe, Y., and Taş, B. (2020). Assessment of stream quality and health risk in a subtropical Turkey river system: a combined approach using statistical analysis and water quality index. *Ecol. Indic.* 113, 105815. doi: 10.1016/j.ecolind.2019.1 05815

Vinnarasi, F., Srinivasamoorthy, K., Saravanan, K., Rajesh Kanna, A., Gopinath, S., Prakash, R., et al. (2022). Hydrogeochemical characteristics and risk evaluation of potential toxic elements in groundwater from Shanmughanadhi, Tamilnadu, India. *Environ. Res.* 204, 112199. doi: 10.1016/j.envres.2021.1 12199

Vlastélic, I., Bougault, H., and Dosso, L. (2002). Heterogeneous heat production in the Earth's upper mantle: blob melting and MORB composition. *Earth Planet. Sci. Lett.* 199, 157–172. doi: 10.1016/S0012-821X(02)00538-1

Wang, J., Zhou, X., He, M., Li, J., Dong, J., Tian, J., et al. (2022). Hydrogeochemical origin and circulation of spring waters along the Karakorum fault, Western Tibetan Plateau: implications for interaction between hydrosphere and lithosphere. *Front. Earth Sci.* 10, 1021550. doi: 10.3389/feart.2022.10 21550

Xiao, C., Liu, J., Liang, X., and Du, S. (2016). Hydrogeochemistry characteristics of groundwater and its suitability for water supply and irrigation in Jilin City, China. *Arab. J. Geosci.* 9, 434. doi: 10.1007/s12517-016-2447-1

Yotova, G., Varbanov, M., Tcherkezova, E., and Tsakovski, S. (2021). Water quality assessment of a river catchment by the composite water quality index and self-organizing maps. *Ecol. Indic.* 120, 106872. doi: 10.1016/j.ecolind.2020.106872

Yousefi, M., Ghoochani, M., and Hossein Mahvi, A. (2018). Health risk assessment to fluoride in drinking water of rural residents living in the Poldasht city, Northwest of Iran. *Ecotoxicol. Environ. Saf.* 148, 426–430. doi: 10.1016/j.ecoenv.2017.10.057

Zhang, C. S., Zhang, Y. C., and Wu, M. L. (2003). Study on relationship between earthquakeand hydro-geochemistry of groundwater in southern part of North-South earthquake belt in China. *J. Geomech.* 9, 21–30. (in Chinese).

Zhang, H., Zhou, X., Wang, L., Wang, W., and Xu, J. (2018). Concentrations and potential health risks of strontium in drinking water from Xi'an, Northwest China. *Ecotoxicol. Environ. Saf.* 164, 181–188. doi: 10.1016/j.ecoenv.2018.08.017

Zhang, Q., Xu, P., and Qian, H. (2020). Groundwater quality assessment using improved Water Quality Index (WQI) and Human Health Risk (HHR) evaluation in a semi-arid region of Northwest China. *Exposure Health* 12, 487–500. doi: 10.1007/s12403-020-00345-w

Zhang, Z., Xiao, C., Yang, W., Adeyeye, O. A., and Liang, X. (2021). Effects of the natural environment and human activities on iron and manganese content in groundwater: a case study of Changchun city, Northeast China. *Environ. Sci. Pollut. Res.* 28, 41109–41119. doi: 10.1007/s11356-021-13576-4

Zhao, D., Zhou, X., Zhang, Y., He, M., Tian, J., Shen, J., et al. (2023). Hydrogeochemical study of hot springs along the Tingri—Nyima Rift: relationship between fluids and earthquakes. *Water* 15, 1634. doi: 10.3390/w15081634

Zhong, C., Wang, H., and Yang, Q. (2022). Hydrochemical interpretation of groundwater in Yinchuan basin using self-organizing maps and hierarchical clustering. *Chemosphere* 309, 136787. doi: 10.1016/j.chemosphere.2022.136787

Zhou, H., Zhou, X., Su, H., Li, Y., Liu, F., Ouyang, S., et al. (2022a). Hydrochemical characteristics of earthquake-related thermal springs along the Weixi–Qiaohou Fault, Southeast Tibet Plateau. *Water* 14, 132. doi: 10.3390/w14010132

Zhou, J., Wu, Q., Gao, S., Zhang, X., Wang, Z., Wu, P., et al. (2023). Coupled controls of the infiltration of rivers, urban activities and carbonate on trace elements in a karst groundwater system from Guiyang, Southwest China. *Ecotoxicol. Environ. Saf.* 249, 114424. doi: 10.1016/j.ecoenv.2022.114424

Zhou, R., Zhou, X., Li, Y., He, M., Li, J., Dong, J., et al. (2022b). Hydrogeochemical and isotopic characteristics of the hot springs in the litang fault zone, Southeast Qinghai–Tibet Plateau. *Water* 14, 1496. doi: 10.3390/w14091496